g_j factor of an electron bound in a hydrogenlike ion

Thomas Beier,* Ingvar Lindgren, Hans Persson, Sten Salomonson, and Per Sunnergren
Department of Physics, Chalmers University of Technology and Göteborg University, S-412 96 Göteborg, Sweden

Hartmut Häffner
GSI, Planckstrasse 1, DE-64 291 Darmstadt, Germany

Nikolaus Hermanspahn
Institut für Physik, Universität Mainz, DE-55 099 Mainz, Germany
(Received 24 January 2000; published 17 August 2000)

We present a detailed theoretical evaluation for the g_j factor of a bound electron in hydrogenlike ions up to $Z=94$. All quantum electrodynamical corrections of order (α/π) are evaluated in detail and various other contributions to the g_j factor are computed and listed for 61 Z. A comparison with all existing experiments is carried out and excellent agreement is found. The present uncertainty in our calculations is discussed. It is not possible to improve this precision with only minor effort since two-photon bound-state QED terms are uncalculated up to now.

PACS number(s): 31.30.Jv, 12.20.−m, 32.10.Fn

I. INTRODUCTION

Currently, enormous effort is undertaken to investigate quantum electrodynamical (QED) effects in the strong fields of highly charged few-electron ions. Experimentally, this implies handling and precise spectroscopy of systems up to U^{91+}. Theoretically, the binding field of the nucleus has to be considered nonperturbatively and must include all orders in $Z\alpha$. In hydrogenlike ions, the theoretical evaluation of many diagrams of order α^2 contributing to the Lamb shift has already been performed [1] and the current theoretical uncertainty amounts to 2 eV in U^{91+}, whereas the most recent measurement agrees well with theory but still has an error of ± 13 eV [2]. For lithiumlike ions, a number of excellent measurements in different heavy systems were performed [3–8], but theoretical predictions still lack a complete treatment of two-photon contributions [9–13]. Also a number of very precise measurements of hyperfine structure splittings in heavy hydrogenlike systems [14–17] and in heavy lithiumlike systems [6] were carried out. Unfortunately, due to insufficient knowledge of nuclear parameters such as the nuclear magnetization distribution the theoretical precision for hyperfine structure predictions is rather poor although it coincides with experiment [18–24].

Another quantity particularly accessible for high precision experiments is the g_j factor of an electron bound in a hydrogenlike system. Theoretical investigations date back to 1928 when Breit performed his calculations on the relativistic spin-orbit coupling for the g factor [25]. The QED corrections to the g factor of a free electron have their own famous history. The computation of the leading correction in (α/π) was already performed by Schwinger in 1947 [26,27], immediately after Kusch and Foleys's legendary experiment [28,29]. Contributions of order $(\alpha/\pi)^2$ were considered by Karplus and Kroll [30] and finally evaluated analytically by Petermann [31] and Sommerfield [32]. The corrections of order $(\alpha/\pi)^3$ comprise already 72 Feynman diagrams which have all been evaluated analytically since 1996 [33]. The most recent overview is given by Hughes and Kinoshita [34] who also present a number of recent theoretical values for the g factor of the free electron, depending on the experimentally measured value of α which is employed. For example, from muonium hyperfine structure measurements [35] $1/\alpha = 137.035\,996\,3(80)$, which leads to $g_{\text{free}} = 2 + 2 \times 1\,159\,652\,216.0(1.2)(67.8) \times 10^{-12}$, where the first error results from the calculations of the $(\alpha/\pi)^4$ terms and from nonelectronic QED and non-QED contributions. The second error is due to the uncertainty in α employed in this calculation. The terms of order $(\alpha/\pi)^4$ comprise 891 diagrams and up to now have only been evaluated numerically.

The by far most precise experimental measurement to date on the g factor of the free electron was performed by Van Dyck *et al.* [36] who obtained a value of $g_{\text{free}} = 2 + 2 \times 1\,159\,652\,188.4(4.3) \times 10^{-12}$. Contrary to this outstanding success, investigations on the QED bound-state modifications to g_j were rather sparse until the mid 1990's. Grotch and Hegstrom [37–39] as well as Faustov [40,41] and Close and Osborn [42] performed calculations on the first terms of a $Z\alpha$ expansion for QED and recoil corrections to g_j. Experiments were carried out on hydrogen and deuterium (Refs. [43–45], and references therein) as well as on He^+ [46]. The existing theoretical calculations were then sufficient to describe the experimental results.

Recently, a new setup was developed [47] and tested [48] which allows the storage of a single hydrogenlike ion in a trap and the performance of g_j measurements with a precision up to a few ppb [49]. At the same time, theoretical results became available which treated the bound-state QED effects nonperturbatively in $Z\alpha$. The self-energy diagrams of order α were calculated by Blundell *et al.* [50] and also by

*Author to whom correspondence should be addressed. Electronic address: f3atb@fy.chalmers.se

Persson *et al.* [51]. Persson *et al.* [51] investigated also the vacuum polarization contributions and were thus the first to publish results which contained the complete QED corrections of order α for a number of Z in the range up to $Z=92$. A detailed presentation of the separate contributions was given only for C^{5+}, S^{15+}, and Ca^{19+} [52], but without a specific presentation of the theoretical calculations. In this work we are going to describe the method employed in Refs. [51,52] in detail. After a short summary on the general theory, we will focus on the QED contributions in particular. Our method in evaluating the diagrams will be presented as well as the numerical techniques we employ. We will also list the other known contributions, i.e., the effects of finite nuclear size and mass, and discuss their uncertainties. Results will be presented for all even Z up to $Z=94$ and also for a few odd Z which are of particular experimental interest due to the possible determination of the g_j factor from hyperfine-transition lifetime measurements [53]. The results will be compared to the sparse experimental values available up to now, and finally we outline what has to be done next to improve the theoretical precision further. Although we present formulas valid for any bound state of an electron, we restrict ourselves in the numerical calculations to the $1s_{1/2}$ state which for high-precision measurements is the most interesting state.

In this work, we generally employ $4\pi\alpha=e^2$ and $\hbar=c=m_e=1$, except when specified otherwise. The electron mass is explicitly specified in some formulas for clarity. Four vectors and their components are given in roman style (p) and have the form $(p_0,\mathbf{p})$, bold letters indicate three vectors and italics denote scalars. Four-dimensional space-time coordinates are denoted by x, y, and z with $x=(t_x,\mathbf{x})$. The Feynman dagger is employed to indicate $\not{p}=\gamma^\mu p_\mu$, and $\hat{\mathbf{p}}=\mathbf{p}/|\mathbf{p}|$.

II. g FACTOR OF AN ELECTRON BOUND IN A HYDROGENLIKE SYSTEM

The g factor of a rotating charge q with mass m_q and angular momentum $\mathbf{J}$ is defined by the ratio of angular momentum and magnetic moment

$$\boldsymbol{\mu}=g_j\frac{q}{2m_q c}\mathbf{J}. \tag{1}$$

For an electron, $q=-e$, and

$$\boldsymbol{\mu}=-g_j\frac{e}{2m_e c}\mathbf{J}=-g_j\mu_B\frac{\mathbf{J}}{\hbar}, \tag{2}$$

where μ_B is the Bohr magneton. Setting $\mathbf{J}=\mathbf{S}$ and using the Dirac equation with minimal coupling of the electromagnetic field, $g_{\rm free}=2$ is readily obtained (a straightforward evaluation is performed, e.g., in Ref. [54]).

For a bound electron, only the total angular momentum $\mathbf{J}$ can be observed. The energy shift of a state $|a_n\rangle$ due to an external magnetic field (for simplicity assumed to point along the z direction) is given by

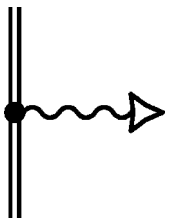

FIG. 1. The interaction of a bound electron (double line) with the external magnetic field (triangle) depicted as a Feynman diagram. The wavy line indicates a photon.

$$\Delta E=-\langle a_n|\boldsymbol{\mu}\cdot\mathbf{B}|a_n\rangle=g_j\frac{\mu_B}{\hbar}B_z\langle a_n|J_z|a_n\rangle=\frac{1}{2}g_j\mu_B B_z \tag{3}$$

for an electron with $|a_n\rangle=|s_{1/2}\rangle$ and magnetic angular quantum number $m=1/2$. This can be also written as

$$\Delta E=\langle a_n|\boldsymbol{\alpha}\cdot e\mathbf{A}|a_n\rangle, \tag{4}$$

where

$$\mathbf{A}=-(\mathbf{r}\times\mathbf{B})/2. \tag{5}$$

It leads to

$$g_j=\frac{e}{\mu_B}\langle a_n|\hat{\mathbf{z}}\cdot(\mathbf{r}\times\boldsymbol{\alpha})|a_n\rangle \tag{6}$$

$$=2\left[\frac{1+2\sqrt{1-(Z\alpha)^2}}{3}\right], \tag{7}$$

where the last equal sign is valid only for an electron bound to a pointlike nucleus. Only in this case is the analytical calculation of all appearing integrals possible. The result is due to Breit [25]. Detailed evaluations of this last equation are performed, e.g., in Refs. [55] and [56]. Equations (6) and (7) describe the deviation of g_j from 2 because of binding only and do not account for any QED effects.

III. QED CORRECTIONS TO THE g_j FACTOR

A. Basic formulas

The basic interaction of a bound electron with the external magnetic field can be envisaged as in Fig. 1. Note that the interaction due to the presence of an external homogeneous magnetic field is always treated as a perturbation because of the smallness of its influence compared to the nuclear binding potential. Quantum electrodynamical corrections can be obtained employing Sucher's symmetrized form [57] of the Gell-Mann–Low level shift [58], presented in detail in Refs. [1,59,60] and applied to one- and few-electron QED corrections extensively also in Refs. [22,50,51,61,62]. From the formulas for the energy shifts, the corresponding expressions for g_j are obtained by the relation (3). In this section, we will restrict ourselves to deal with the formulas for the energy shift.

In general, the energy shift for a single-electron system is given by

$$\Delta E_n = \lim_{\substack{\epsilon\to 0\\ \lambda\to 1}} \frac{i\epsilon\lambda}{2} \frac{\frac{\partial}{\partial\lambda}\langle n|S_{\epsilon,\lambda}|n\rangle}{\langle n|S_{\epsilon,\lambda}|n\rangle} \tag{8}$$

with

$$S_{\epsilon,\lambda} = T\left\{\exp\left[-i\lambda\int dx e^{-\epsilon|t_x|} H_I(x)\right]\right\}. \tag{9}$$

The basic interaction between the electron-positron field and the photon field is described by the interaction Hamiltonian (e.g., Refs. [1,59,63]),

$$H_I(x) = j^\mu(x)[A_\mu(x) + A^{\rm pert}_\mu(x)] \tag{10}$$

$$= H_I^A + H_I^B. \tag{11}$$

Here,

$$j^\mu(x) = -\frac{1}{2} e[\overline{\psi}(x)\gamma^\mu, \psi(x)] \tag{12}$$

is the Dirac current operator, $A_\mu(x)$ is the quantized field photon operator, and $A^{\rm pert}$ denotes the additional magnetic perturbing potential not considered for binding. In Eq. (9), T denotes the time-ordering symbol. To evaluate this expression, Wick's theorem [64] is commonly applied which allows one to rewrite the time-ordered product of a number of operators into a sum of normal-ordered products with all possible contractions. The special case of two Fermion operators with equal times requires some care in bound state problems. Contrary to QED of free fermions, these terms have to be retained as they lead to the vacuum polarization corrections [59].

Equation (8) is evaluated into powers of λ, which yields

$$\lim_{\lambda\to 1} \frac{\frac{\partial}{\partial\lambda}\langle n|S_{\epsilon,\lambda}|n\rangle}{\langle n|S_{\epsilon,\lambda}|n\rangle}$$

$$= \frac{\langle n|S_\epsilon^{(1)}|n\rangle + 2\langle n|S_\epsilon^{(2)}|n\rangle + 3\langle n|S_\epsilon^{(3)}|n\rangle + \cdots}{1 + \langle n|S_\epsilon^{(1)}|n\rangle + \langle n|S_\epsilon^{(2)}|n\rangle + \langle n|S_\epsilon^{(3)}|n\rangle + \cdots}$$

$$= \langle n|S_\epsilon^{(1)}|n\rangle + 2\langle n|S_\epsilon^{(2)}|n\rangle - \langle n|S_\epsilon^{(1)}|n\rangle^2 + 3\langle n|S_\epsilon^{(3)}|n\rangle$$

$$- 3\langle n|S_\epsilon^{(1)}|n\rangle\langle n|S_\epsilon^{(2)}|n\rangle + \langle n|S_\epsilon^{(1)}|n\rangle^3 + \cdots. \tag{13}$$

Performing all contractions, only those terms of each order in λ are retained in Eq. (13) which describe connected graphs, i.e., do not consist of more than one disjunct diagram. In addition, only expressions meaningful to the current problem are considered. As we deal with one electron only, this excludes contraction results with more than one fermion in the initial and final state. Furthermore, only terms with all operators $A_\mu(x)$ of the quantized photon field contracted will be considered [60]. Finally, we keep only terms which are of first order in the perturbing potential $A^{\rm pert}$ and of order α, which indicates one virtual photon line in a diagram. Therefore, it is sufficient to include summands up to $S_\epsilon^{(3)}$, where the different orders in λ read

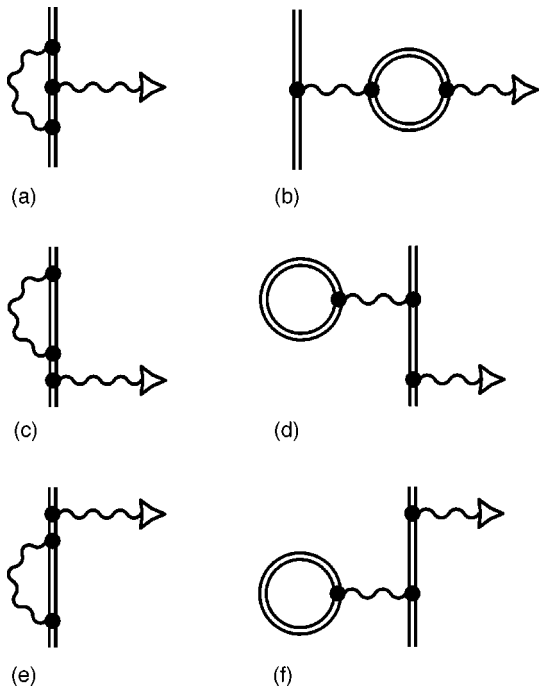

FIG. 2. The QED contributions of order (α/π) to the bound-electron g_j factor depicted as Feynman diagrams.

$$S_\epsilon^{(1)} = (-i\lambda)\int dx e^{-\epsilon|t_x|} T[(H_I^B(x)], \tag{14}$$

$$S_\epsilon^{(2)} = \frac{(-i\lambda)^2}{2}\int dy \int dx e^{-\epsilon|t_y|} e^{-\epsilon|t_x|} T\{[H_I^A(y) H_I^A(x)]\}, \tag{15}$$

$$S_\epsilon^{(3)} = \frac{(-i\lambda)^3}{3!}\int dz \int dy \int dx e^{-\epsilon|t_z|} e^{-\epsilon|t_y|} e^{-\epsilon|t_x|}$$

$$\times T\{[H_I^B(z) H_I^A(y) H_I^A(x)] + [H_I^A(z) H_I^B(y) H_I^A(x)]$$

$$+ [H_I^A(z) H_I^A(y) H_I^B(x)]\}. \tag{16}$$

Equation (15) yields the well-known expressions for the first-order self energy and vacuum polarization [59,61]. The three terms in Eq. (16) yield all the same result as the contractions can be carried out for each in the same way. Six different expressions are obtained which can be envisaged by Fig. 2. In Ref. [59], the mass counterterm is also integrated into the formalism of Eqs. (8)–(11). It is sufficient, however, to introduce this term explicitly when needed in order to keep the general formulas simpler. A detailed derivation for the mass counterterm in connection with the first-order QED terms is performed in Ref. [59].

The terms for the diagrams of Fig. 2 read

$$\Delta E_{\rm SE,ve} = \lim_{\epsilon\to 0} \frac{i\epsilon}{2} 3 S^{(3)}_{\rm SE,ve}, \tag{17}$$

$$\Delta E_{\rm SE,WF} = \lim_{\epsilon\to 0} \frac{i\epsilon}{2} [3 S^{(3)}_{\rm SE,WF} - 3 S^{(1)} S^{(2)}_{\rm SE}], \tag{18}$$

$$\Delta E_{\mathrm{VP,pot}} = \lim_{\epsilon\to 0} \frac{i\epsilon}{2} 3S^{(3)}_{\mathrm{VP,pot}}, \tag{19}$$

$$\Delta E_{\mathrm{VP,WF}} = \lim_{\epsilon\to 0} \frac{i\epsilon}{2} [3S^{(3)}_{\mathrm{VP,WF}} - 3S^{(1)}S^{(2)}_{\mathrm{VP}}], \tag{20}$$

where the indices refer to the self-energy vertex term, Fig. 2(a), the self-energy wave function correction terms, Figs. 2(c) and 2(e), the vacuum polarization potential term Fig. 2(b), and the vacuum polarization wave function correction terms Figs. 2(d) and 2(f). The self-energy vertex term and the vacuum polarization potential term form irreducible diagrams. These diagrams can be evaluated directly by employing the bound-state Feynman rules as presented, e.g., by Lindgren [61,62] which can be shown to be equivalent to a full evaluation in the *S* matrix formalism. The same holds for the irreducible contribution of the wave function corrections, i.e., the part of the expression where the energy of the intermediate state between magnetic interaction and self-energy loop does not conincide with that of the state under consideration. The other part we term ''reducible'' contribution. In the Feynman gauge, the irreducible self-energy contributions read

$$\begin{aligned}\Delta E_{\mathrm{SE,ve}} = e^2 \frac{i}{2\pi} \int d\mathbf{x} \int d\mathbf{y} \int d\mathbf{z} \\ \times \int d\omega \overline{a}_n(\mathbf{y}) \gamma^\mu D_{F\mu\nu}(\mathbf{y},\mathbf{x},\omega) \\ \times S_F(\mathbf{y},\mathbf{z},E_n-\omega) e\boldsymbol{\gamma}\cdot\mathbf{A}(\mathbf{z}) \\ \times S_F(\mathbf{z},\mathbf{x},E_n-\omega)\gamma^\nu a_n(\mathbf{x}),\end{aligned} \tag{21}$$

$$\begin{aligned}\Delta E_{\mathrm{SE,WF,irred}} = 2e^2 \frac{i}{2\pi} \int d\mathbf{x} \int d\mathbf{y} \int d\mathbf{z} \int d\omega \overline{a}_n(\mathbf{y})\gamma^\mu \\ \times D_{F\mu\nu}(\mathbf{y},\mathbf{x},\omega) \\ \times S_F(\mathbf{y},\mathbf{x},E_n-\omega)\gamma^\nu \\ \times \sum_{\substack{q \\ E_q\neq E_n}} \frac{\Phi_q(\mathbf{x})\Phi_q^\dagger(\mathbf{z})\gamma^0}{E_n-E_q} e\boldsymbol{\gamma}\cdot\mathbf{A}(\mathbf{z}) a_n(\mathbf{z}) \\ = 2 \sum_{\substack{q \\ E_q\neq E_n}} \frac{\langle a_n|\gamma^0\Sigma(E_n)|\Phi_q\rangle\langle\Phi_q|e\boldsymbol{\alpha}\cdot\mathbf{A}|a_n\rangle}{E_n-E_q},\end{aligned} \tag{22}$$

where the self-energy operator $\Sigma(E_n)$ was introduced,

$$\begin{aligned}\langle a|\gamma^0\Sigma(E)|b\rangle = e^2 \frac{i}{2\pi} \int d\mathbf{x} \int d\mathbf{y} \int d\omega \overline{a}(\mathbf{y})\gamma^\mu \\ \times D_{F\mu\nu}(\mathbf{y},\mathbf{x},\omega) S_F(\mathbf{y},\mathbf{x},E-\omega)\gamma^\nu b(\mathbf{x}).\end{aligned} \tag{23}$$

In Eq. (22), an additional factor 2 accounts for the two symmetrical diagrams Figs. 2(c) and 2(e). In all these equations, $S_F(\mathbf{x},\mathbf{y};E)\gamma_0$ denotes the time-independent Green's function of a bound electron

$$\{E - [\boldsymbol{\alpha}\cdot\mathbf{p} + \beta m + V^{\mathrm{bind}}_{\mathrm{nuc}}(\mathbf{x})]\} S_F(\mathbf{x},\mathbf{y};E)\gamma_0 = \delta^3(\mathbf{x}-\mathbf{y}). \tag{24}$$

Note that our definition coincides with that of Refs. [13,50,65] and differs from Mohr's [1,59,66] by a minus sign in the denominator of $S_F(\mathbf{x},\mathbf{y};E)$. The time-independent Green's function is related to the four-dimensional electron propagator by

$$\begin{aligned}S_F(\mathrm{x},\mathrm{y}) &= \frac{i}{2\pi} \int dE e^{-i(t_x-t_y)E} \sum_m \frac{\Phi_m(\mathbf{x})\overline{\Phi}_m(\mathbf{y})}{E-E_m(1-i\eta)} \\ &= \frac{i}{2\pi} \int dE e^{-i(t_x-t_y)E} S_F(\mathbf{x},\mathbf{y};E).\end{aligned} \tag{25}$$

In the Feynman gauge, the photon propagator $D_{F\mu\nu}(\mathrm{x},\mathrm{y})$ reads

$$D_{F\mu\nu}(\mathrm{x},\mathrm{y}) = -g_{\mu\nu} \frac{1}{(2\pi)^4} \int d\mathbf{k} \int d\omega \frac{e^{-i\omega(t_x-t_y)} e^{i\mathbf{k}(\mathbf{x}-\mathbf{y})}}{\omega^2 - \mathbf{k}^2 + i\eta} \tag{26}$$

$$= \int \frac{d\omega}{2\pi} e^{-i\omega(t_x-t_y)} D_{F\mu\nu}(\mathbf{x},\mathbf{y},\omega). \tag{27}$$

Note that Mohr [1,59] includes an additional i in this definition. For the eigenstates of the Dirac Hamiltonian with the binding potential $V^{\mathrm{bind}}_{\mathrm{nuc}}$ present, the notations Φ_m, Φ_q, etc., are employed, where m,q, etc., are cumulative quantum numbers. The corresponding energy eigenvalues are denoted by E_m, E_q, ... To separate the state under consideration clearly from the intermediate states, we denote it by a_n, where n is again a cumulative quantum number, $a_n \equiv \Phi_n$, and $\overline{a_n}(\mathbf{x}) = a_n^\dagger(\mathbf{x})\gamma^0$.

The vacuum polarization contributions read

$$\begin{aligned}\Delta E_{\mathrm{VP,pot}} = -e^2 \frac{i}{2\pi} \int d\mathbf{x} \int d\mathbf{y} \int d\mathbf{z} D_{F\mu\nu}(\mathbf{x},\mathbf{y},\omega=0) \\ \times \int_{-\infty}^{\infty} dE \overline{a}_n(\mathbf{x})\gamma^\mu a_n(\mathbf{x}) \,\mathrm{Tr}\,[\gamma^\nu S_F(\mathbf{y},\mathbf{z};E) \\ \times e\boldsymbol{\gamma}\cdot\mathbf{A}(\mathbf{z}) S_F(\mathbf{z},\mathbf{y};E)].\end{aligned} \tag{28}$$

$$\Delta E_{\mathrm{VP,WF,irred}} = 2 \sum_{\substack{q \\ E_q\neq E_n}} \frac{\langle a_n|U_{\mathrm{VP}}|\Phi_q\rangle\langle\Phi_q|e\boldsymbol{\alpha}\cdot\mathbf{A}|a_n\rangle}{E_n-E_q}. \tag{29}$$

Again, the symmetry of two equally contributing diagrams was taken into account by an additional factor 2 in Eq. (29). The vacuum polarization potential introduced in Eq. (29) reads

$$U_{\rm VP}(\mathbf{x}) = -e^2 \frac{i}{2\pi} \int d\mathbf{y} D_{F00}(\mathbf{x},\mathbf{y},\omega=0) \times \int dE\, {\rm Tr}\left[\sum_r \frac{\Phi_r(\mathbf{y})\Phi_r^\dagger(\mathbf{y})}{E - E_r(1-i\eta)} \right]. \quad (30)$$

A detailed derivation of the vacuum polarization potential is given by Refs. [66,67], and references therein.

The reducible parts can be treated in a similar manner as for the photon exchange diagrams in few-electron systems [61,68–71], taking into account that the magnetic potential under investigation here replaces the perturbing potential of another electron in the corresponding formulas. To handle the additional singularity in one of the electron propagators, caused by $1/(E_n - E_n)$, the remaining electron propagator of the self-energy diagrams is evaluated around $E = E_n - \omega$. The leading term of this expansion cancels with the corresponding product of lower order terms $S^{(1)} S^{(2)}_{\rm SE}$. After the transition $\epsilon \to 0$ the remaining term formally contains a derivative of the self-energy operator [71]. In an equivalent manner, this term can also be obtained as a perturbation of the binding energy caused by the influence of an external potential [22,72,73] or by employing the two-times Green's function method [65]. It reads

$$\Delta E_{\rm SE,WF,red} = \left\langle a_n \left| \gamma^0 \frac{\partial}{\partial E} \Sigma(E) \right|_{E=E_n} \right| a_n \right\rangle \langle a_n | e\boldsymbol{\alpha}\cdot\mathbf{A} | a_n \rangle \quad (31)$$

for states which are only degenerate in their magnetic quantum number, i.e., in particular for the $1s_{1/2}$ state. For the vacuum polarization wave function correction, no dependence on the energy of the state under consideration exists, except in the electron propagator itself which is mediating between the magnetic interaction and the vacuum polarization vertex. Any expansion similar to the self-energy does not yield any derivative terms, and the reducible part of $S^{(3)}_{\rm VP,WF}$ is completely cancelled by the product $S^{(1)} S^{(2)}_{\rm VP}$ and has not to be considered further. The index ''irred'' will therefore be dropped in the following on vacuum polarization terms.

B. Divergences

The expressions (21), (22), (31), (28), and (29) for the diagrams 2(a), 2(c) and 2(e), 2(b), and 2(d) and 2(f) are only formal. They contain divergences and therefore require renormalization. Our way to deal with the divergences of the self energy expressions is to evaluate the bound-state electron propagators into powers of the nuclear binding potential and to isolate the mass and charge divergences which are present in the lowest order terms only. These terms are treated analytically in momentum space, and after cancelling the divergences between different diagrams a finite result is obtained. The finite higher-order terms are evaluated in coordinate space by employing the full yet unrenormalized expression and subtracting the divergent lower-order parts in the calculation. The procedure outlined so far coincides with

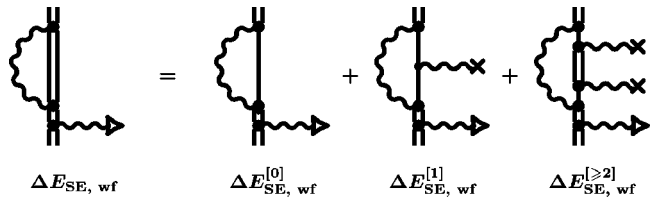

FIG. 3. The decomposition of $\Delta E_{\rm SE,WF,irred}$ into terms appropriate for removing divergences and for numerical calculation. A photon line terminated by a cross denotes one interaction with the nuclear binding potential $V^{\rm bind}_{\rm nuc}$. The labels under the diagrams correspond to the expressions used in the text. For brevity the index ''irred'' was omitted on all labels.

that employed by Snyderman [74] and has been described in detail in Ref. [22] for the QED corrections to the hyperfine structure splitting.

The decomposition of the irreducible part of the self-energy wave function correction term is depicted in Fig. 3. The divergent terms are these with zero and one interaction in the binding potential present, below referred to as ''zero-potential term'' and ''one-potential term,'' respectively. The charge divergences cancel between both terms, as we are going to show. In addition, a mass counter term δm has to be subtracted to obtain proper mass renormalization similar to the case of the free self-energy [75] (for our schemes see also Ref. [76]).

Throughout our work we employ the Feynman gauge, which yields for the free self-energy operator ($E = {\rm p}_0$ here, the dependence on $\mathbf{p}$ is not explicitly indicated)

$$\Sigma^{[0]}(E) = -ie^2 \int \frac{d{\rm k}}{(2\pi)^4} \gamma^\mu \frac{\not{\rm p} - \not{\rm k} + m_e}{({\rm p}-{\rm k})^2 - m_e^2} \gamma_\mu \frac{1}{{\rm k}^2}. \quad (32)$$

(We denote the number of interactions with the binding potential by superscript numbers in brackets.) This operator contains a mass and a charge divergence which are also present in the expression (22). The mass renormalized free self-energy operator reads [74]

$$\Sigma^{[0]}_{\rm mass\ ren}(E) = \Sigma^{[0]}(E) - \delta m = -\frac{e^2}{(4\pi)^2} \left\{ (\not{\rm p} - m_e) \left[\Delta + 2 + \frac{\rho}{1-\rho} \left(1 + \frac{2-\rho}{1-\rho} \ln\rho \right) \right] + \frac{m_e \rho}{1-\rho} \left(1 - \frac{2-3\rho}{1-\rho} \ln\rho \right) \right\}, \quad (33)$$

where

$$\rho = -\frac{(\not{\rm p} - m_e)(\not{\rm p} + m_e)}{m_e^2}. \quad (34)$$

By $\Delta = 2/\epsilon - \gamma_E + \ln 4\pi$ we denote the ultraviolet part of the charge renormalization constant after dimensional regularization where ϵ denotes the dimensional regularization pa-

rameter and γ_E is Euler's constant. The full expression for the charge renormalization constant Z_2 reads (e.g., Ref. [63])

$$Z_2-1=\left.\frac{\partial\Sigma(E)}{\partial\not{p}}\right|_{\not{p}=m_e}=\left.-\frac{\alpha}{4\pi}[\Delta+4+4\ln\rho]\right|_{\rho\to 0}, \tag{35}$$

where the logarithmic term represents the gauge-dependent infrared divergence which would be absent in the Fried-Yennie gauge but can be shown to cancel in the total expression for the wave function correction. Therefore, care has to be taken comparing our intermediate numerical results with other calculations. However, the final value of $\Delta E_{\mathrm{SE,WF,irred}}$ is well defined, and we will not consider the infrared divergent term any more in the following. The expression for the total zero-potential term reads

$$\Delta E^{[0]}_{\mathrm{SE,WF,\ irred}}=2\langle a_n|\gamma^0\Sigma^{[0]}_{\mathrm{mass\text{-}ren}}(E)|\delta a_n\rangle, \tag{36}$$

where

$$|\delta a_n\rangle=\sum_{\substack{q\\ E_q\neq E_n}}\frac{|\Phi_q\rangle\langle\Phi_q|e\boldsymbol{\alpha}\cdot\mathbf{A}|a_n\rangle}{E_n-E_q}. \tag{37}$$

To express the one-potential term, it is advantageous to introduce the vertex operator for a free electron,

$$\Gamma^{[0]}_{\mu}(\mathrm{p},\mathrm{p}')=-ie^2\int\frac{d\mathrm{k}}{(2\pi)^4}\gamma^{\nu}\frac{\not{p}-\not{k}+m_e}{(\mathrm{p}-\mathrm{k})^2-m_e^2}\times\gamma_{\mu}\frac{\not{p}'-\not{k}+m_e}{(\mathrm{p}'-\mathrm{k})^2-m_e^2}\gamma_{\nu}\frac{1}{\mathrm{k}^2}. \tag{38}$$

A representation of Γ_0 in Feynman gauge is presented in Appendix A.

The complete expression related to $\Delta E^{[1]}_{\mathrm{SE,WF,irred}}$ can be expressed as

$$\Delta E^{[1]}_{\mathrm{SE,WF,\ irred}}=2\langle a_n|\gamma^0\Gamma^{[0]}_0(\mathrm{p},\mathrm{p}')V^{\mathrm{bind}}_{\mathrm{nuc}}(\mathbf{p},\mathbf{p}')|\delta a_n\rangle, \tag{39}$$

where $V^{\mathrm{bind}}_{\mathrm{nuc}}(\mathbf{p},\mathbf{p}')$ denotes the Fourier transform of the nuclear binding potential,

$$V^{\mathrm{bind}}_{\mathrm{nuc}}(q)=-\frac{Z\alpha}{2\pi^2q^2}+\frac{1}{2\pi^2}\int_0^{R_0}drr^2j_0(qr)\left[V^{\mathrm{bind}}_{\mathrm{nuc}}(r)-\left(-\frac{Z\alpha}{r}\right)\right] \tag{40}$$

with $\mathbf{q}=\mathbf{p}-\mathbf{p}', q=|\mathbf{q}|, r=|\mathbf{r}|$. R_0 denotes the smallest radius value, for which no difference between the employed potential for an extended nucleus and the $1/r$ Coulomb potential is found. According to the Fourier transform of the Dirac equation

$$(\not{p}-m_e)a(\mathbf{p})=\int d\mathbf{p}'\gamma^0V^{\mathrm{bind}}_{\mathrm{nuc}}(\mathbf{p},\mathbf{p}')a(\mathbf{p}') \tag{41}$$

the cancellation between the terms containing Δ in Eqs. (36) and (39) becomes obvious when adding these terms. In the following, we denote therefore by $\Sigma^{[0]}_R(E)-\delta m$ and $\Gamma^{[0]}_{R0}(\mathrm{p},\mathrm{p}')$ the expression (33) and the zeroth component of Eq. (38) with the divergent part due to Δ omitted (see Appendix A). The other components of $\Gamma^{[0]}_{\mu}(\mathrm{p},\mathrm{p}')$ will be discussed together with $\Delta E_{\mathrm{SE,ve}}$.

The remaining contribution $\Delta E^{[\geqslant 2]}_{\mathrm{SE,WF,\ irred}}$ is obtained by employing

$$\Sigma^{[\geqslant 2]}(E)=\Sigma^{\mathrm{bound}}(E)-[\Sigma^{[0]}(E)+\Sigma^{[1]}(E)], \tag{42}$$

where all Σ on the right-hand side denote unrenormalized operators. The divergences present in the expression (22) are thus explicitly subtracted and therefore cancelled.

The complete finite expression for the wave function correction reads

$$\Delta E_{\mathrm{SE,WF,irred}}=2\langle a_n|\gamma^0[\Sigma^{[0]}_R(E_n)-\delta m+\Gamma^{[0]}_{R0}(\mathrm{p},\mathrm{p}')V_C(\mathbf{p},\mathbf{p}')+\Sigma^{[\geqslant 2]}(E_n)]|\delta a_n\rangle. \tag{43}$$

The reducible part of the self-energy wave function correction, Eq. (31), also contains an ultraviolet divergent part which is cancelled by a similar expression present in the vertex correction term, Eq. (21). In addition, an infrared divergence exists which mutually cancels as well. These two terms are therefore evaluated together. Both contributions are decomposed into a zero-potential term with the full electron propagators within the loop replaced by free ones, and the remaining ''many-potential'' part.

To obtain $\partial\Sigma^{[0]}_{\mathrm{mass\ ren}}(E)/\partial E$, Eq. (33) is differentiated with respect to $\mathrm{p}_0=E$ which yields

$$\frac{\partial\Sigma^{[0]}(E)}{\partial E}=-\frac{e^2}{(4\pi)^2}\left\{\gamma_0\left[\Delta+2+\frac{\rho}{1-\rho}\left(1+\frac{2-\rho}{1-\rho}\ln\rho\right)\right]+\frac{\not{p}}{m_e^2}\left[-\frac{2E}{(1-\rho)^2}\left(3-\rho+\frac{2}{1-\rho}\ln\rho\right)\right]+\frac{8E}{m_e(1-\rho)}\left[1+\frac{1}{1-\rho}\ln\rho\right]\right\} \tag{44}$$

The energy-independent mass renormalization term has not to be considered in this differentiation. However, again this expression contains the ultraviolet part of the renormalization constant which can be explicitly separated,

$$\Delta E^{[0]}_{\mathrm{SE,WF,red}}=\left[\left\langle a_n\left|\gamma^0\frac{\partial}{\partial E}\Sigma^{[0]}_R(E)\right|_{E=E_n}\right|a_n\right\rangle-\frac{e^2}{(4\pi)^2}\Delta\right]\times\langle a_n|e\boldsymbol{\alpha}\cdot\mathbf{A}|a_n\rangle. \tag{45}$$

It is cancelled out by the part of the vertex correction with the free vertex function present,

$$\begin{aligned}\Delta E^{[0]}_{\mathrm{SE,ve}} &= \langle a_n | e\gamma^0 \mathbf{\Gamma}^{[0]}(\mathrm{p},\mathrm{p}')\mathbf{A}(\mathbf{p},\mathbf{p}')|a_n\rangle \\ &= \langle a_n | e\gamma^0 \mathbf{\Gamma}^{[0]}_R(\mathrm{p},\mathrm{p}')\mathbf{A}(\mathbf{p},\mathbf{p}')|a_n\rangle \\ &\quad + \frac{e^2}{(4\pi)^2}\Delta\langle a_n | e\boldsymbol{\alpha}\cdot\mathbf{A}|a_n\rangle, \end{aligned} \tag{46}$$

where

$$\mathbf{A}(\mathbf{q}) = \frac{i}{2}\boldsymbol{\nabla}_{\mathbf{q}}\delta^3(\mathbf{q})\times\mathbf{B} \tag{47}$$

is the Fourier transform of the magnetic potential and $\mathbf{q}=\mathbf{p}-\mathbf{p}'$. The terms containing interactions with the binding potential $\Delta E^{[\geq 1]}_{\mathrm{SE,ve}}$ and $\Delta E^{[\geq 1]}_{\mathrm{SE,WF,red}}$, contain no ultraviolet divergences and are evaluated similarly to the irreducible wave function correction by subtracting the unrenormalized free contributions from the also unrenormalized full contributions, Eqs. (21) and (31).

Techniques for removing the divergences present in the vacuum polarization expressions (28) and (29) exist on a broad scale, as the modification of the photon propagator due to a vacuum polarization loop is a rather common feature within QED. The potential U_{VP} present in Eq. (29) is the same as that appearing in QED calculations related to the Lamb shift and therefore its already renormalized expression can be taken from other work [66,67,77,78]. The charge divergence is introduced by the leading term of the expansion in the nuclear potential. One standard technique to remove it is to apply a Pauli-Villars regularization technique (Ref. [79], see also Ref. [80]). The potential remaining after the charge renormalization, $U^{\mathrm{Ueh}}_{\mathrm{VP}}$, is commonly termed Uehling potential [81] and reads

$$\begin{aligned}U^{\mathrm{Ueh}}_{\mathrm{VP}}(r) = -Z\left(\frac{e^2}{4\pi}\right)^2\frac{2}{3}\int_0^\infty dr' r'\rho(r')\int_1^\infty dt \\ \times\left(1+\frac{1}{2t^2}\right)\frac{\sqrt{t^2-1}}{t^2}\,\frac{e^{-2(|r-r'|)t}-e^{-2(|r+r'|)t}}{rt},\end{aligned} \tag{48}$$

where $r=|\mathbf{r}|, r'=|\mathbf{r}'|$. $Ze\rho(r')$ represents the charge distribution of a spherically symmetric nucleus, $\int d\mathbf{r}'\rho(r')=1$. Numerical evaluations can be found in numerous works [82–86], and all modern calculations of vacuum polarization contributions to one- [66,67,77,87] and few-electron [71,78,88,89] Lamb shift calculations employ this form.

The remaining part, the Wichmann-Kroll potential, also contains a spurious gauge-dependent piece [87] which can be easily removed by the partial wave expansion common in that evaluation [66,67]. Equation (29) is decomposed into

$$\begin{aligned}\Delta E_{\mathrm{VP,wf}} &= 2\left\{\sum_{\substack{q\\ E_q\neq E_n}}\frac{\langle a_n|U^{\mathrm{Ueh}}_{\mathrm{VP}}|\Phi_q\rangle\langle\Phi_q|e\boldsymbol{\alpha}\cdot\mathbf{A}|a_n\rangle}{E_n-E_q}\right. \\ &\quad \left. + \sum_{\substack{q\\ E_q\neq E_n}}\frac{\langle a_n|U^{\mathrm{WK}}_{\mathrm{VP}}|\Phi_q\rangle\langle\Phi_q|e\boldsymbol{\alpha}\cdot\mathbf{A}|a_n\rangle}{E_n-E_q}\right\} \\ &= \langle a_n|U^{\mathrm{Ueh}}_{\mathrm{VP}}|\,\delta a_n\rangle + \langle a_n|U^{\mathrm{WK}}_{\mathrm{VP}}|\,\delta a_n\rangle \\ &= \Delta E^{\mathrm{Ueh}}_{\mathrm{VP,WF}} + \Delta E^{\mathrm{WK}}_{\mathrm{VP,WF}}.\end{aligned} \tag{49}$$

A similar expansion is applied for $\Delta E_{\mathrm{VP,pot}}$. Note, that the terms containing one interaction with the nuclear Coulomb field vanish due to Furry's theorem [90]. The leading term is known as the Uehling part of the magnetic loop. In momentum space, it reads

$$\begin{aligned}\Delta E^{\mathrm{Ueh}}_{\mathrm{VP,pot}} = \int d\mathbf{p}\int d\mathbf{p}'\,\overline{a_n}(\mathbf{p})[-e^2\Pi^{\mathrm{ren}}(|\mathbf{p}-\mathbf{p}'|^2)] \\ \times e\boldsymbol{\gamma}\cdot\mathbf{A}(\mathbf{p}-\mathbf{p}')a_n(\mathbf{p}')\end{aligned} \tag{50}$$

where the (already renormalized) polarization function $-e^2\Pi^{\mathrm{ren}}(|\mathbf{p}-\mathbf{p}'|^2)$ accounts for the polarization loop in the photon line [91]. It is given by

$$e^2\Pi^{\mathrm{ren}}(\mathbf{q}^2) = -\frac{e^2}{4\pi^2}\int_1^\infty dt\sqrt{t^2-1}\left(\frac{2}{3t^2}+\frac{1}{3t^4}\right)\frac{\mathbf{q}^2}{\mathbf{q}^2+4m_e^2t^2} \tag{51}$$

which reads for small $\mathbf{q}$

$$e^2\Pi^{\mathrm{ren}}(\mathbf{q}^2) = -\frac{e^2}{4\pi^2}\left[\frac{1}{15}\left(\frac{\mathbf{q}^2}{m_e^2}\right)-\frac{1}{140}\left(\frac{\mathbf{q}^2}{m_e^2}\right)^2+O(\mathbf{q}^6)\right]. \tag{52}$$

This leads to a value of $\Delta E^{\mathrm{Ueh}}_{\mathrm{VP,pot}}=0$ for the case under consideration here, as becomes clear from the Fourier transform of the potential of a constant external magnetic field, Eq. (47), which leads to

$$\begin{aligned}\Delta E^{\mathrm{Ueh}}_{\mathrm{VP,pot}} = \frac{i}{2}\int d\mathbf{p}\int d\mathbf{p}'\,\overline{a_n}(\mathbf{p})[-e^2\Pi^{\mathrm{ren}}(|\mathbf{p}-\mathbf{p}'|^2)] \\ \times e\boldsymbol{\gamma}\cdot[\boldsymbol{\nabla}_{\mathbf{p}}\delta^3(\mathbf{p}-\mathbf{p}')\times\mathbf{B}]a_n(\mathbf{p}').\end{aligned} \tag{53}$$

By partial integration, $\Delta E^{\mathrm{Ueh}}_{\mathrm{VP,pot}}=0$ is obvious, and therefore also the vanishing contribution to g_j. The remaining part is finite except for a spurious gauge dependent piece which also can be shown to vanish by applying a proper partial wave decomposition [78].

C. Calculation formulas

After removing all divergences, we present the formulas actually employed in our calculations here. We start with the contributions to $\Delta E_{\mathrm{SE,WF,irred}}$, which are closely related to the expressions for the self-energy correction of order α to the Lamb shift, presented in Ref. [74]. From Eq. (33), the tensor structure of $\Sigma^{[0]}_{\mathrm{R}}(E)-\delta m$ can be expressed as $a(\rho)+\not{p}b(\rho)$. The wave function a_n reads in momentum space

$$a_n(\mathbf{p}) = \frac{1}{(2\pi)^{3/2}} \int d\mathbf{r} e^{-i\mathbf{p}\cdot\mathbf{r}} a_n(\mathbf{r}) = \begin{pmatrix} P_{a_n}(p)\chi^m_\kappa(\hat{\mathbf{p}}) \\ Q_{a_n}(p)\chi^m_{-\kappa}(\hat{\mathbf{p}}) \end{pmatrix}, \tag{54}$$

where $p=|\mathbf{p}|$, $P(p)$ and $Q(p)$ depend only on $|\mathbf{p}|$, and $\chi^m_\kappa(\hat{\mathbf{p}})$ is the ls coupled spin-angular function in momentum space (e.g., Ref. [56]). Considering

$$\boldsymbol{\sigma}\cdot\hat{\mathbf{p}}\chi^m_\kappa(\hat{\mathbf{p}}) = -\chi^m_{-\kappa}(\hat{\mathbf{p}}), \tag{55}$$

$$\Delta E^{[0]}_{\mathrm{SE,WF,\,irred}} = 2\int dp p^2 [C(p)a(\rho) + D(p)b(\rho)] \tag{56}$$

after carrying out the angular integrations. The functions $C(p)$ and $D(p)$ are given by

$$C(p) = P_{a_n}(p)P_{\delta a_n}(p) - Q_{a_n}(p)Q_{\delta a_n}(p), \tag{57}$$

$$\begin{aligned} D(p) = {} & E[P_{a_n}(p)P_{\delta a_n}(p) + Q_{a_n}(p)Q_{\delta a_n}(p)] \\ & + p[P_{a_n}(p)Q_{\delta a_n}(p) + P_{\delta a_n}(p)Q_{a_n}(p)]. \end{aligned} \tag{58}$$

Equation (56) can be evaluated numerically employing a Gauss-Legendre quadrature.

Equation (39) for $\Delta E^{[1]}_{\mathrm{SE,WF,\,irred}}$ is evaluated by

$$\begin{aligned} \Delta E^{[1]}_{\mathrm{SE,WF,irred}} = 2\int d\mathbf{p} d\mathbf{p}' a^\dagger_n(\mathbf{p})\gamma^0 [& \gamma_0 f_1(p,p',\cos\vartheta) \\ & + \not{p} f_2(p,p',\cos\vartheta) + \not{p}' f_3(p,p',\cos\vartheta) \\ & + \not{p}\gamma_0\not{p}' f_4(p,p',\cos\vartheta) \\ & + f_5(p,p',\cos\vartheta)] V^{\mathrm{bind}}_{\mathrm{nuc}}(\mathbf{p},\mathbf{p}')\,\delta a_n(\mathbf{p}'), \end{aligned} \tag{59}$$

where ϑ denotes the angle between $\mathbf{p}$ and $\mathbf{p}'$ and $V^{\mathrm{bind}}_{\mathrm{nuc}}(\mathbf{p},\mathbf{p}')$ is given by Eq. (40). The f_i are abbreviations for the coefficient functions in Eq. (A1) in Appendix A. The spherically symmetric nuclear potential $V^{\mathrm{bind}}_{\mathrm{nuc}}$ does not depend on angular variables except $\cos\vartheta$ and therefore the tensor structure of Eq. (59) can be reduced into an expression of functions of $\cos\vartheta$, p, and p'. This yields

$$\begin{aligned} a^\dagger_n(\mathbf{p})\gamma_0\Gamma^{[0]}_{R,0}(p,p')\,\delta a_n(\mathbf{p}') = \frac{1}{4\pi}(& f_1(p,p',\cos\vartheta)[P_{a_n}(p)P_{\delta a_n}(p') + Q_{a_n}(p)Q_{\delta a_n}(p')\cos\vartheta] + f_2(p,p',\cos\vartheta) \\ & \times\{E_n P_{a_n}(p)P_{\delta a_n}(p') + pQ_{a_n}(p)P_{\delta a_n}(p') + [pP_{a_n}(p)Q_{\delta a_n}(p') \\ & + E_n Q_{a_n}(p)Q_{\delta a_n}(p')]\cos\vartheta\} + f_3(p,p',\cos\vartheta)\{E_n P_{a_n}(p)P_{\delta a_n}(p') + p'P_{a_n}(p)Q_{\delta a_n}(p') \\ & + [p'Q_{a_n}(p)P_{\delta a_n}(p') + E_n Q_{a_n}(p)Q_{\delta a_n}(p')]\cos\vartheta\} + f_4(p,p',\cos\vartheta)\{E_n^2 P_{a_n}(p)P_{\delta a_n}(p') \\ & + pE_n Q_{a_n}(p)P_{\delta a_n}(p') + p'E_n P_{a_n}(p)Q_{\delta a_n}(p') + pp'Q_{a_n}(p)Q_{\delta a_n}(p') \\ & + [pp'P_{a_n}(p)P_{\delta a_n}(p') + pE_n P_{a_n}(p)Q_{\delta a_n}(p') + p'E_n Q_{a_n}(p)P_{\delta a_n}(p') \\ & + E_n^2 Q_{a_n}(p)Q_{\delta a_n}(p')]\cos\vartheta\} + f_5(p,p',\cos\vartheta)[P_{a_n}(p)P_{\delta a_n}(p') - Q_{a_n}(p)Q_{\delta a_n}(p')\cos\vartheta]), \end{aligned} \tag{60}$$

for the $1s_{1/2}$ state. From Eq. (60), a numerical integration of Eq. (59) over p, p', and $\cos\vartheta$ is possible employing some variable transformations suggested by Blundell [92]. For the self-energy contribution to the Lamb shift, a related decomposition was also recently performed in Ref. [93].

The remaining contribution $\Delta E^{[\geq 2]}_{\mathrm{SE,WF,irred}}$ is obtained as specified by Eq. (42). Performing the integrations over ω and the angular part of $\mathbf{k}$, Eq. (22) reads

$$\Delta E_{\mathrm{SE,WF,irred}} = -\frac{e^2}{2\pi^2}\sum_{l=0}^{\infty}(2l+1)\int dk k \sum_p \frac{\langle a_n|\alpha^\mu j_l(ky)\mathbf{C}^l(\hat{\mathbf{y}})|\Phi_p\rangle\langle\Phi_p|\alpha_\mu j_l(kx)\mathbf{C}^l(\hat{\mathbf{x}})|\,\delta a_n\rangle}{E_n - E_p - \mathrm{sgn}(E_p)k}, \tag{61}$$

where $k=|\mathbf{k}|, x=|\mathbf{x}|, y=|\mathbf{y}|$. A spherical wave expansion was employed according to

$$\frac{\sin(k|\mathbf{y}-\mathbf{x}|)}{k|\mathbf{y}-\mathbf{x}|} = \sum_{l=0}^{\infty}(2l+1)\mathbf{C}^l(\hat{\mathbf{y}})\cdot\mathbf{C}^l(\hat{\mathbf{x}})j_l(ky)j_l(kx), \tag{62}$$

where j_l denotes a spherical Bessel function and $\mathbf{C}^l(\hat{\mathbf{x}})$ is a spherical tensor operator (e.g., Ref. [94]), defined by

$$C^l_m(\hat{\mathbf{x}}) = \sqrt{\frac{4\pi}{(2l+1)}}Y^m_l(\hat{\mathbf{x}}). \tag{63}$$

$Y^l_m(\hat{\mathbf{x}})$ denotes a spherical harmonic. The scalar product between two tensor operators $\mathbf{C}^l(\hat{\mathbf{y}})\cdot\mathbf{C}^l(\hat{\mathbf{x}})$ reads

$$\mathbf{C}^l(\hat{\mathbf{y}})\cdot\mathbf{C}^l(\hat{\mathbf{x}})=\sum_{m=-l}^{l}(-1)^m C^l_m(\hat{\mathbf{y}})C^l_{-m}(\hat{\mathbf{x}}). \tag{64}$$

This scalar product is implicitly assumed in all formulas with $\mathbf{C}^l$ present in two matrix elements.

To obtain the unrenormalized contribution from the term due to the free self-energy operator, a similar evaluation is carried out, but the bound-state electron propagator S_F in Eq. (22) is replaced by that for free electrons. In the final result the sum over the spectrum of the bound state Dirac equation $\Sigma_p|\Phi_p\rangle\langle\Phi_p|$ is replaced by one over the spectrum of the Dirac equation without an additional potential, $\Sigma_r|\varphi_r\rangle\langle\varphi_r|$, where we use small Greek letters for denoting the eigenfunctions of the free Dirac Hamiltonian. In the same manner, the contribution for the free vertex part (the one-potential term) is obtained by replacing the bound-state propagators in the full vertex expression [see formula (78) below] by free-state propagators. The total result for the subtraction scheme reads

$$\begin{aligned}\Delta E^{[\geqslant 2]}_{\mathrm{SE,WF,\,irred}}=&-\frac{e^2}{2\pi^2}\sum_{l=0}^{\infty}(2l+1)\int dkk\Bigg\{\sum_p\frac{\langle a_n|\alpha^\mu j_l(ky)\mathbf{C}^l(\hat{\mathbf{y}})|\Phi_p\rangle\langle\Phi_p|j_l(kx)\mathbf{C}^l(\hat{\mathbf{x}})\alpha_\mu|\delta a_n\rangle}{E_n-E_p-\mathrm{sgn}(E_p)k}\\&-\sum_r\frac{\langle a_n|\alpha^\mu j_l(ky)\mathbf{C}^l(\hat{\mathbf{y}})|\varphi_r\rangle\langle\varphi_r|j_l(kx)\mathbf{C}^l(\hat{\mathbf{x}})\alpha_\mu|\delta a_n\rangle}{E_n-E_r-\mathrm{sgn}(E_r)k}\\&-\sum_{s,r}\frac{\langle a_n|\alpha^\mu j_l(ky)\mathbf{C}^l(\hat{\mathbf{y}})|\varphi_s\rangle\langle\varphi_s|V^{\mathrm{bind}}_{\mathrm{nuc}}|\varphi_r\rangle\langle\varphi_r|j_l(kx)\mathbf{C}^l(\hat{\mathbf{x}})\alpha_\mu|\delta a_n\rangle}{[E_n-E_s-\mathrm{sgn}(E_s)k][E_n-E_r-\mathrm{sgn}(E_r)k]}F(s,r)\Bigg\}.\end{aligned} \tag{65}$$

The function F is introduced here to denote part of the energy denominator

$$F(s,r)=1+[\mathrm{sgn}(E_r)-\mathrm{sgn}(E_s)]\frac{k}{E_r-E_s}. \tag{66}$$

If E_n represents the lowest positive energy eigenvalue of the bound Dirac spectrum, the further evaluation of Eq. (65) is straightforward employing standard methods. In the present work this is the case and we do not have to consider any singularities caused by zeros of the denominator. If $|a_n\rangle\neq|1s_{1/2}\rangle$, due to positive values of E_q with $E_q<E_n$, singularities on the integration path for k appear. The corresponding principal value integrals can be carried out employing a polynomial approximation of the numerator for obtaining the real part of the contribution. The imaginary part which is also present in such a case does not contribute to the energy shift but only to the line width of the excited state in a one-electron ion (Ref. [60], and references therein) which is not under consideration here. We will therefore omit the corresponding discussion here and also in the related cases of the other k integrals of this work.

For the expression in curly braces, we separate radial and angular integrations and carry out the latter utilizing the graphical angular momentum coupling scheme as presented by Lindgren *et al.* [69,94,95]. Writing down an explicit formula containing all details, the wave function $|\delta a\rangle$ also has to be considered. The angular structure is identical for the three sums over the states present in Eq. (65) and yields $\kappa_q=-1$. Equation (65) can therefore be written as

$$\begin{aligned}\Delta E^{[\geqslant 2]}_{\mathrm{SE,WF,\,irred}}=&-\frac{e^2}{2\pi^2}\left\langle\frac{eB_z}{2}\right\rangle\sum_{l=0}^{\infty}(2l+1)\int dkk\sum_{\substack{s\\E_q\neq E_n}}\frac{2\kappa_q}{4\kappa_q-1}\mathcal{R}(n,q)\Bigg\{\sum_p\frac{1}{(E_n-E_q)[E_n-E_p-\mathrm{sgn}(E_p)k]}\\&\times[\mathcal{A}^0_{\mathrm{SE}}(n,p;l)\mathcal{S}(n,p,p,q;k,l)+\mathcal{A}^1_{\mathrm{SE}}(n,p;l)\mathcal{V}^1(n,p,p,q;k,l)+\mathcal{A}^2_{\mathrm{SE}}(n,p;l)\mathcal{V}^2(n,p,p,q;k,l)\\&+\mathcal{A}^3_{\mathrm{SE}}(n,p;l)\mathcal{V}^3(n,p,p,q;k,l)+\mathcal{A}^4_{\mathrm{SE}}(n,p;l)\mathcal{V}^4(n,p,p,q;k,l)]\\&-\sum_r{}^{(\mathrm{free})}\frac{1}{(E_n-E_q)[E_n-E_r-\mathrm{sgn}(E_r)k]}[\mathcal{A}^0_{\mathrm{SE}}(n,r;l)\mathcal{S}(n,r,r,q;k,l)+\mathcal{A}^1_{\mathrm{SE}}(n,r;l)\mathcal{V}^1(n,r,r,q;k,l)\\&+\mathcal{A}^2_{\mathrm{SE}}(n,r;l)\mathcal{V}^2(n,r,r,q;k,l)+\mathcal{A}^3_{\mathrm{SE}}(n,r;l)\mathcal{V}^3(n,r,r,q;k,l)+\mathcal{A}^4_{\mathrm{SE}}(n,r;l)\mathcal{V}^4(n,r,r,q;k,l)]\\&-\sum_{s,r}{}^{(\mathrm{free})}\frac{F(s,r)}{(E_n-E_q)(E_n-E_s-\mathrm{sgn}(E_s)k)[E_n-E_r-\mathrm{sgn}(E_r)k]}[\mathcal{A}^0_{\mathrm{SE}}(n,r;l)\mathcal{T}(n,s,r,q;k,l)\\&+\mathcal{A}^1_{\mathrm{SE}}(n,r;l)\mathcal{W}^1(n,s,r,q;k,l)+\mathcal{A}^2_{\mathrm{SE}}(n,r;l)\mathcal{W}^2(n,s,r,q;k,l)+\mathcal{A}^3_{\mathrm{SE}}(n,r;l)\mathcal{W}^3(n,s,r,q;k,l)\\&+\mathcal{A}^4_{\mathrm{SE}}(n,r;l)\mathcal{W}^4(n,s,r,q;k,l)]\Bigg\}.\end{aligned} \tag{67}$$

The angular factors $\mathcal{A}_{\mathrm{SE}}$ are given in Appendix B. For the radial integrals $\mathcal{R}$, $\mathcal{S}$, $\mathcal{T}$, $\mathcal{V}$, and $\mathcal{W}$, expressions are presented in Appendix C. For the last term containing the additional interaction with the nuclear potential, no particular angular factor occurs as the spherically symmetric potential $V_{\mathrm{nuc}}^{\mathrm{bind}}$ demands strictly identical angular quantum numbers for φ_s and φ_r.

The sums over intermediate bound and free states are carried out by generating a complete set of intermediate states utilizing the space-discretization method of Salomonson and Öster [96]. The functions obtained by this method are given on a few finite sets of grid points only. The integrations are also carried out on the same grids, if the grid sizes prove to be sufficient for an accurate calculation which is controlled by extrapolating the number of grid points to infinity. For high k, the spherical Bessel functions are strongly oscillating, and therefore the grid-valued functions have to be interpolated to continuous space using Lagrange polynomials [76] to obtain the proper values of the matrix elements.

The outer k integration is handled numerically, using Gauss-Legendre and Gauss-Laguerre quadrature formulas. Finally, the sum over l is carried out by evaluating a finite number of summands and performing a polynomial expansion to infinity. For the correction under consideration here, the summands up to $l \leqslant 30$ can be evaluated without problems for most (except very low) Z.

Now the different contributions of $(\Delta E_{\mathrm{SE,ve}} + \Delta E_{\mathrm{SE,WF,red}})$ are analyzed. The term which contains the derivation of the free self-energy operator $\partial \Sigma_R^{[0]}(E)/\partial E$, exhibits a tensor structure similar to that of $\Sigma_R^{[0]}(E) - \delta m$ itself,

$$\frac{\partial \Sigma_R^{[0]}(E)}{\partial E} = \frac{\partial a(\rho)}{\partial E} + \not{p} \frac{\partial b(\rho)}{\partial E} + \gamma^0 b(\rho). \tag{68}$$

This leads to

$$\begin{aligned}\Delta E_{\mathrm{SE,WF,red}}^{[0]} = \langle a_n | e \boldsymbol{\alpha} \cdot \mathbf{A} | a_n \rangle \int dp p^2 \\ \times \Bigg[[P_{a_n}^2(p) - Q_{a_n}^2(p)] \frac{\partial a(\rho)}{\partial E} \\ + \{ E_n [P_{a_n}^2(p) + Q_{a_n}^2(p)] \\ + 2pP_{a_n}(p) Q_{a_n}(p) \} \frac{\partial b(\rho)}{\partial E} \\ + [P_{a_n}^2(p) + Q_{a_n}^2(p)] b(\rho) \Bigg]_{E=E_n}\end{aligned} \tag{69}$$

[cf. Eq. (56)], where all angular integrations are carried out in Eq. (69). This equation is then numerically evaluated similarly to Eq. (56). $\Delta E_{\mathrm{SE,ve}}^{[0]}$ reads

$$\begin{aligned}\Delta E_{\mathrm{SE,ve}}^{[0]} &= \langle a_n | e \gamma^0 \boldsymbol{\Gamma}_R^{[0]}(p,p') \cdot \mathbf{A}(\mathbf{p},\mathbf{p}') | a_n \rangle \\ &= e^3 \int d\mathbf{p} \int d\mathbf{p}' \overline{a_n}(\mathbf{p}) \\ &\quad \times \{ \boldsymbol{\gamma} g_1(p,p',\cos\vartheta) + \not{p} [\mathbf{p} g_2(p,p',\cos\vartheta) \\ &\quad + \mathbf{p}' g_3(p,p',\cos\vartheta)] + \not{p}' [\mathbf{p} g_4(p,p',\cos\vartheta) \\ &\quad + \mathbf{p}' g_5(p,p',\cos\vartheta)] + \mathbf{p} g_6(p,p',\cos\vartheta) \\ &\quad + \mathbf{p}' g_7(p,p',\cos\vartheta) + \not{p} \boldsymbol{\gamma} \not{p}' \\ &\quad \times g_8(p,p',\cos\vartheta) \} \cdot \mathbf{A}(\mathbf{p}-\mathbf{p}') a_n(\mathbf{p}'),\end{aligned} \tag{70}$$

where the g_i are again abbreviations for the coefficient functions in Eq. (A1). However, the evaluation of Eq. (70) is not as straightforward as that of Eq. (59) as the angular dependency is contained in the potential $\mathbf{A}(\mathbf{p}-\mathbf{p}')$ as well. Formally, $\mathbf{A}(\mathbf{p}-\mathbf{p}')$ is given by Eq. (47). To obtain an expression suitable for numerical evaluation, a Gaussian cutoff is introduced in coordinate space

$$\mathbf{r} \rightarrow \lim_{\varrho \rightarrow 0} \mathbf{r} e^{-(\varrho |\mathbf{r}|/2)} \tag{71}$$

which leads to a smoothing in momentum space

$$\mathbf{A}(\mathbf{q}) = \frac{i}{\pi^{3/2} \varrho^5} e^{-(|\mathbf{q}|/\varrho)^2} \mathbf{q} \times \mathbf{B}. \tag{72}$$

The value of ϱ is then chosen to be small enough to guarantee homogeneity of the magnetic field over the extension of the ion.

The exponential in Eq. (72) can also be expressed in terms of p, p', and $\cos\vartheta$ $(\mathbf{q}=\mathbf{p}-\mathbf{p}')$. The complete angular dependency can be separated out by using

$$e^{-(|\mathbf{p}-\mathbf{p}'|/\varrho)^2} \stackrel{\mathrm{def}}{=} V^{\exp}(p,p',\cos\vartheta), \tag{73}$$

and

$$V^{\exp}(p,p',\cos\vartheta) = \sum_{l=0}^{\infty} (2l+1) V_l^{\exp}(p,p') \mathbf{C}^l(\hat{\mathbf{p}}) \cdot \mathbf{C}^l(\hat{\mathbf{p}}'), \tag{74}$$

where the evaluation coefficients read

$$V_l^{\exp}(p,p') = \tfrac{1}{2} \int_{-1}^{1} d\cos\vartheta V^{\exp}(p,p',\cos\vartheta) P_l(\cos\vartheta). \tag{75}$$

P_l denotes the Legendre polynomial of order l. The remaining part of $\mathbf{A}$ is linear in $\mathbf{p}$ and $\mathbf{p}'$ and enters Eq. (70) by simple vector multiplication. Thus, Eq. (70) contains only terms linear in $\mathbf{p}$ and $\mathbf{p}'$ and expressions of p, p', and $\cos\vartheta$. The angular integrations are again carried out employing the graphical angular momentum coupling scheme mentioned already [69,94]. A detailed derivation is given in Ref. [97]. The remaining integrals over p, p', and $\cos\vartheta$ are evaluated numerically.

The expressions $\Delta E^{[\geqslant 1]}_{\mathrm{SE,ve}}$ and $\Delta E^{[\geqslant 1]}_{\mathrm{SE,WF,red}}$ are obtained in the same manner as $\Delta E^{[\geqslant 2]}_{\mathrm{SE,WF,red}}$, namely, by subtracting the unrenormalized free parts from the corresponding unrenormalized bound expressions. From Eq. (61), $\langle a_n|\gamma^0[\partial\Sigma(E)/\partial E]_{E=E_n}|a_n\rangle$ is obtained by replacing $|\delta a_n\rangle$ with $|a_n\rangle$ and differentiating with respect to the energy of the state under consideration. This holds true for both the bound and the free expressions, and therefore

$$\Delta E^{[\geqslant 1]}_{\mathrm{SE,WF,red}}=\langle a_n|e\boldsymbol{\alpha}\cdot\mathbf{A}|a_n\rangle\times\frac{e^2}{4\pi^2}\sum_{l=0}^{\infty}(2l+1)\int dkk\Bigg\{\sum_p\frac{\langle a_n|\alpha^\mu j_l(ky)\mathbf{C}^l(\hat{\mathbf{y}})|\Phi_p\rangle\langle\Phi_p|j_l(kx)\mathbf{C}^l(\hat{\mathbf{x}})\alpha_\mu|a_n\rangle}{[E_n-E_p-\mathrm{sgn}(E_p)k]^2}$$
$$-\sum_r\frac{\langle a_n|\alpha^\mu j_l(ky)\mathbf{C}^l(\hat{\mathbf{y}})|\varphi_r\rangle\langle\varphi_r|j_l(kx)\mathbf{C}^l(\hat{\mathbf{x}})\alpha_\mu|a_n\rangle}{[E_n-E_r-\mathrm{sgn}(E_r)k]^2}\Bigg\} \tag{76}$$

As already mentioned, the first term is infrared divergent for $l=0$ and $\mu=0$, if the energy of the intermediate state p coincides with E_n. A similar term with opposite sign occurs from the vertex term which will be discussed next. Therefore the sum of both terms is infrared finite. In performing their numerical evaluation, we explicitly exclude the terms with $l=0,\mu=0$ from the calculation. The detailed decomposition of the matrix elements in Eq. (76) into radial and angular parts is rather similar to that of Eq. (65). A number of simplifications occur, as the magnetic interaction part is totally factorized out. The remaining product of two matrix elements is identical to that of the self energy of order α which has been considered before [76,98]. Explicitly displayed, the first product of the matrix elements in Eq. (76) reads

$$\langle a_n|\alpha^\mu j_l(ky)\mathbf{C}^l(\hat{\mathbf{y}})|\Phi_p\rangle\langle\Phi_p|j_l(kx)\mathbf{C}^l(\hat{\mathbf{x}})\alpha_\mu|a_n\rangle=\mathcal{A}^0_{\mathrm{SE}}(n,p;l)\mathcal{S}(n,p,p,n;k,l)+\mathcal{A}^1_{\mathrm{SE}}(n,p;l)\mathcal{V}^1(n,p,p,n;k,l)$$
$$+\mathcal{A}^2_{\mathrm{SE}}(n,p;l)\mathcal{V}^2(n,p,p,n;k,l)+\mathcal{A}^3_{\mathrm{SE}}(n,p;l)\mathcal{V}^3(n,p,p,n;k,l)$$
$$+\mathcal{A}^4_{\mathrm{SE}}(n,p;l)\mathcal{V}^4(n,p,p,n;k,l) \tag{77}$$

and the second one accordingly, with p replaced by r, and free instead of bound-state functions employed in the radial expressions for $\mathcal{S}$ (C3) and $\mathcal{V}^i$ (C5)–(C8). The angular factors are the same as those in Eq. (67). They are given in Appendix B. Note, that the sum over Φ_q in Eq. (67) is replaced by the state under consideration $|a_n\rangle$ here.

The vertex contribution is obtained by evaluating Eq. (21) in a manner similar to Eq. (22),

$$\Delta E_{\mathrm{SE,ve}}=-\frac{e^2}{4\pi^2}\sum_{l=0}^{\infty}(2l+1)\int dkk\sum_{q,r}\frac{\langle a_n|a^\mu j_l(ky)\mathbf{C}^l(\hat{\mathbf{y}})|\Phi_q\rangle\langle\Phi_q|e\boldsymbol{\alpha}\cdot\mathbf{A}|\Phi_r\rangle\langle\Phi_r|a_\mu j_l(kx)\mathbf{C}^l(\hat{\mathbf{x}})|a_n\rangle}{[E_n-E_q-\mathrm{sgn}(E_q)k][E_n-E_r-\mathrm{sgn}(E_r)k]}F(q,r), \tag{78}$$

Replacing the magnetic vector potential by the nuclear Coulomb potential and the sums over the bound state eigenfunctions by those of free states, the one-potential subtraction term in Eq. (65) is also obtained. The function F is given by Eq. (66).

Equation (78) is infrared divergent in the same way as Eq. (76) but with different sign. The two divergences cancel therefore and the sum of Eqs. (76) and (78) is infrared finite. Both terms contain ultraviolet divergences which are removed by subtracting terms with free electron propagators instead of the bound ones, as discussed in the previous section. The final expression for evaluating the many-potential part of the vertex correction therefore reads

$$\Delta E^{[\geqslant 1]}_{\mathrm{SE,ve}}=-\frac{e^2}{4\pi^2}\sum_{l=0}^{\infty}(2l+1)\int dkk\Bigg\{\sum_{q,r}\frac{\langle a_n|a^\mu j_l(ky)\mathbf{C}^l(\hat{\mathbf{y}})|\Phi_q\rangle\langle\Phi_q|e\boldsymbol{\alpha}\cdot\mathbf{A}|\Phi_r\rangle\langle\Phi_r|a_\mu j_l(kx)\mathbf{C}^l(\hat{\mathbf{x}})|a_n\rangle}{[E_n-E_q-\mathrm{sgn}(E_q)k][E_n-E_r-\mathrm{sgn}(E_r)k]}F(q,r)$$
$$-\sum_{p,s}\frac{\langle a_n|a^\mu j_l(ky)\mathbf{C}^l(\hat{\mathbf{y}})|\varphi_p\rangle\langle\varphi_p|e\boldsymbol{\alpha}\cdot\mathbf{A}|\varphi_s\rangle\langle\varphi_s|a_\mu j_l(kx)\mathbf{C}^l(\hat{\mathbf{x}})|a_n\rangle}{[E_n-E_p-\mathrm{sgn}(E_p)k][E_n-E_s-\mathrm{sgn}(E_s)k]}F(p,s)\Bigg\}. \tag{79}$$

In analogy to Eq. (67), this expression can be explicitly written as

$$\Delta E_{\mathrm{SE,ve}}^{[\geqslant 1]} = -\frac{e^2}{4\pi^2}\left(\frac{1}{2}eB_z\right)\sum_{l=0}^{\infty}(2l+1)\int dkk$$
$$\times\Bigg\{\sum_{q,r}\frac{F(q,r)\mathcal{R}(q,r)}{[E_n-E_q-\mathrm{sgn}(E_q)k][E_n-E_r-\mathrm{sgn}(E_r)k]}$$
$$\times[\mathcal{A}_{\mathrm{VE}}^{0}(n,q,r;l)\mathcal{S}(n,q,r,n;k,l)+\mathcal{A}_{\mathrm{VE}}^{1}(n,q,r;l)\mathcal{V}^{1}(n,q,r,n;k,l)$$
$$+\mathcal{A}_{\mathrm{VE}}^{2}(n,q,r;l)\mathcal{V}^{2}(n,q,r,n;k,l)+\mathcal{A}_{\mathrm{VE}}^{3}(n,q,r;l)\mathcal{V}^{3}(n,q,r,n;k,l)+\mathcal{A}_{\mathrm{VE}}^{4}(n,q,r;l)\mathcal{V}^{4}(n,q,r,n;k,l)]$$
$$-\sum_{p,s}^{(\mathrm{free})}\frac{F(p,s)\mathcal{R}(p,s)}{[E_n-E_p-\mathrm{sgn}(E_p)k][E_n-E_s-\mathrm{sgn}(E_s)k]}$$
$$\times[\mathcal{A}_{\mathrm{VE}}^{0}(n,p,s;l)\mathcal{S}(n,p,s,n;k,l)+\mathcal{A}_{\mathrm{VE}}^{1}(n,p,s;l)\mathcal{V}^{1}(n,p,s,n;k,l)+\mathcal{A}_{\mathrm{VE}}^{2}(n,p,s;l)\mathcal{V}^{2}(n,p,s,n;k,l)$$
$$+\mathcal{A}_{\mathrm{VE}}^{3}(n,p,s;l)\mathcal{V}^{3}(n,p,s,n;k,l)+\mathcal{A}_{\mathrm{VE}}^{4}(n,p,s;l)\mathcal{V}^{4}(n,p,s,n;k,l)]\Bigg\} \tag{80}$$

The radial integrals are given by Eqs. (C3)–(C8). The angular coefficients were evaluated by Schneider [95] and are presented in Appendix B. In our numerical calculations, the expressions (76) and (79) are computed together within the outer k integration. The partial wave expansion is carried out in the same way as described for the irreducible part of the wave function correction, taking into account that numerical stability is reached only for $l\leqslant 20$. For $Z<20$, however, a sufficient precision could not be reached within this l range. An extension to higher l is currently prevented by the numerical accuracy of our code. Therefore the terms containing one interaction with the nuclear Coulomb potential were also subtracted from Eqs. (76) and (79) and separately evaluated. In terms of Feynman diagrams, this refers to an explicit calculation of the graphs shown in Fig. 4. The expressions for the diagrams under consideration are

$$\Delta E_{\mathrm{SE,ve}}^{[1]} = -2\frac{e^2}{2\pi^2}\sum_{l=0}^{\infty}(2l+1)\int dkk^2\sum_{s,t,u}\langle a_n|a^{\mu}j_l(ky)\mathbf{C}^l(\hat{\mathbf{y}})|\varphi_s\rangle\langle\varphi_s|e\boldsymbol{\alpha}\cdot\mathbf{A}|\varphi_t\rangle$$
$$\times\langle\varphi_t|V_{\mathrm{nuc}}^{\mathrm{bind}}|\varphi_u\rangle\langle\varphi_u|a_{\mu}j_l(kx)\mathbf{C}^l(\hat{\mathbf{x}})|a_n\rangle G(s,t,u) \tag{81}$$

(taking into account two equally contributing diagrams) and

$$\Delta E_{\mathrm{SE,WF,red}}^{[1]} = 2\langle a_n|e\boldsymbol{\alpha}\cdot\mathbf{A}|a_n\rangle\times\frac{e^2}{4\pi^2}\sum_{l=0}^{\infty}(2l+1)\int dkk$$
$$\times\sum_{s,t}\frac{\langle a_n|\alpha^{\mu}j_l(ky)\mathbf{C}^l(\hat{\mathbf{y}})|\varphi_s\rangle\langle\varphi_s|V_{\mathrm{nuc}}^{\mathrm{bind}}|\varphi_t\rangle\langle\varphi_t|j_l(kx)\mathbf{C}^l(\hat{\mathbf{x}})\alpha_{\mu}|a_n\rangle}{[E_n-E_s-\mathrm{sgn}(E_s)k][E_n-E_t-\mathrm{sgn}(E_t)k]^2}F(s,t). \tag{82}$$

Equation (82) was obtained by deriving the last term of Eq. (65). The two arising summands are equal and thus we present only the second of them multiplied by a factor of 2. Equation (81) is derived from the last line of Eq. (79) by inserting one additional interaction with the nuclear Coulomb potential. The structure of the denominator becomes quite complicated for the case of three intermediate states and is therefore contained in the function $G(s,t,u)$ given in Appendix D.

The further angular reduction of Eqs. (81) and (82) is carried out in the same manner as for the corresponding expressions (70) and (59), respectively, as the additional Coulomb interaction does not change the angular structure. In the evaluation of the radial parts it is advantageous to perform the necessary integrations on analytically given free-electron intermediate states. Here we employ free spherical waves given by

$$\varphi_E(\mathbf{r}) = \frac{1}{r}\begin{pmatrix} F_{E,\kappa}(pr)\chi_{\kappa}^{m}(\hat{\mathbf{r}}) \\ iG_{E,\kappa}(pr)\chi_{-\kappa}^{m}(\hat{\mathbf{r}})\end{pmatrix}, \tag{83}$$

where κ is the Dirac angular momentum quantum number, $E=\pm\sqrt{m_e^2+\mathbf{p}^2}$,

$$F_{E,\kappa}(pr) = \sqrt{\frac{|E|+m_e}{\pi|E|}}pr\; j_l(pr), \tag{84}$$

$$G_{E,\kappa}(pr) = \mathrm{sgn}(E)\mathrm{sgn}(\kappa)\sqrt{\frac{|E|-m_e}{\pi|E|}}pr\; j_{l'}(pr), \tag{85}$$

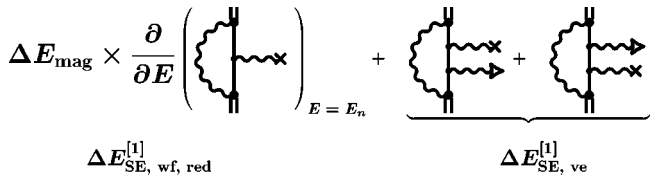

FIG. 4. The terms of $\Delta E_{\mathrm{SE,WF,red}}$ and $\Delta E_{\mathrm{SE,ve}}$ which are of first order in the nuclear Coulomb potential. For $Z<20$, these terms are calculated separately to obtain a better partial wave convergence. ΔE_{mag} denotes the matrix element $\langle a_n|e\boldsymbol{\alpha}\cdot\mathbf{A}|a_n\rangle$.

$$l=|1/2+\kappa|-1/2, \tag{86}$$

$$l'=|1/2-\kappa|-1/2. \tag{87}$$

The summations $\Sigma_{s,t,u}$ which are due to the grid representation of a finite number of intermediate states are thus replaced by integrations. Furthermore, we also expand the state $|a_n\rangle$ under consideration into free spherical waves, denoted by $\langle a_n|\varpi\rangle$. Expression (81) therefore reads

$$\begin{aligned}\Delta E^{[1]}_{\mathrm{SE,ve}}=&-2\frac{e^2}{2\pi^2}\sum_{l=0}^{\infty}(2l+1)\\&\times\int dkk^2\int ds\int dt\int du\int d\varpi\int d\varpi'\\&\times\langle a_n|\varpi\rangle\langle\varpi|a^\mu j_l(ky)\mathbf{C}^l(\hat{\mathbf{y}})|\varphi_s\rangle\langle\varphi_s|e\boldsymbol{\alpha}\cdot\mathbf{A}|\varphi_t\rangle\\&\times\langle\varphi_t|V^{\mathrm{bind}}_{\mathrm{nuc}}|\varphi_u\rangle\langle\varphi_u|a_\mu j_l(kx)\mathbf{C}^l(\hat{\mathbf{x}})|\varpi'\rangle\\&\times\langle\varpi'|a_n\rangle G(s,t,u),\end{aligned} \tag{88}$$

and a similar expansion can be applied to Eq. (82). The radial integration of $\langle a_n|\varpi\rangle$ is performed numerically employing a Lagrange interpolation between the stored values of $|a_n\rangle$ on the grid. To have access to all momenta ϖ of the evaluation, the overlap integral is calculated for a grid of momenta, stored, and interpolated as needed.

The radial parts of the matrix elements containing α^μ and α_μ consist now of a product of three spherical Bessel functions which can be further evaluated analytically. Employing the point nucleus Coulomb potential $-Z\alpha/r$, this also holds true for the matrix element containing $V^{\mathrm{bind}}_{\mathrm{nuc}}$. As the described additional separation is performed for low Z, the nuclear size effect itself is small and the replacement of the actual binding potential by that of a point nucleus is reasonable.

The magnetic potential is treated in parts in momentum space, observing that

$$\langle\varphi_s|\boldsymbol{\alpha}\cdot\mathbf{A}(\mathbf{r})|\varphi_t\rangle=\left\langle\varphi_s\left|\int d^3q e^{i\mathbf{q}\cdot\mathbf{r}}\boldsymbol{\alpha}\cdot\mathbf{A}(\mathbf{q})\right|\varphi_t\right\rangle \tag{89}$$

$$\propto\int dqq^2\mathbf{A}(q)\langle\varphi_{s\ \mathrm{radial}}|j_1(qr)|\varphi_{t\ \mathrm{radial}}\rangle \tag{90}$$

for $\mathbf{A}$ given by Eq. (72). In the inner radial matrix element, the r integration can be carried out again over a product of three spherical Bessel functions. Due to the analytical treatment of most of the matrix elements in Eq. (88) and in the according expression for $\Delta E^{[1]}_{\mathrm{SE,WF,red}}$, the numerical stability is much better for higher l which allows the inclusion of more terms. With the described separation scheme, a proper extrapolation can be obtained even in the cases of hydrogen and helium, where terms up to $l\leqslant 180$ have to be considered.

Let us now turn to the vacuum polarization expressions. The Uehling potential contained in Eq. (49) also represents the major influence of the vacuum polarization on Lamb shift calculations. The first part of Eq. (49) is straightforward to evaluate by carrying out the sum over the intermediate states. Note that the angular structure of the states has to be the same as that of $|a_n\rangle$ ($\kappa=-1$ here) which simplifies the calculation even further.

The remaining part of Eq. (49) is of similar type. The potential, commonly known as Wichmann-Kroll potential after its first investigators Wichmann and Kroll [99], is obtained either in an expansion in $Z\alpha$ which is not applicable for the problem under consideration here [83], or as a difference between the unrenormalized full expression and the also unrenormalized Uehling potential by which any divergences cancel. This procedure is equal to the technique applied for the self energy terms above and was discussed for the vacuum polarization of order α in detail in Ref. [67]. We present therefore only the final expression which reads

$$\begin{aligned}U^{\mathrm{WK}}_{\mathrm{VP}}(\mathbf{x})=&-\frac{e^2}{4\pi^2}\sum_{\kappa=\pm1}^{\pm\infty}(2j_\kappa+1)\int_0^\infty dkj_0(kx)\\&\times\Bigg[\sum_{r,\kappa}\mathrm{sgn}(E_{r,\kappa})\langle\Phi_{r,\kappa}|j_0(ky)|\Phi_{r,\kappa}\rangle\\&-4\sum_{\substack{s\\E_s>0}}\sum_{\substack{t\\E_t<0}}\frac{\langle\varphi_{s,\kappa}|j_l(ky)|\varphi_{t,\kappa}\rangle\langle\varphi_{t,\kappa}|V^{\mathrm{bind}}_{\mathrm{nuc}}|\varphi_{s,\kappa}\rangle}{E_s-E_t}\Bigg].\end{aligned} \tag{91}$$

Only electron-positron pairs contribute to the vacuum polarization loop, and therefore the sums over s and t can be restricted to positive and negative energies, respectively, for calculation purposes. An additional factor of 2 accounts for this.

A remaining gauge-dependent spurious term [87,99,100] can be shown to disappear for each finite κ [66]. In the same manner as for the l expansions for the self-energy contributions, the sum over κ is carried out to a maximum value of $|\kappa_{\mathrm{max}}|$ which includes both κ_{max} and $-\kappa_{\mathrm{max}}$, and therefore the spurious term causes no difficulties. The maximal value of $|\kappa|$ in our calculations permitted by numerical stability is about 30.

The potential correction is handled in a similar manner. As shown already, the leading Uehling term yields zero for a homogeneous external magnetic field. The remaining Wichmann-Kroll term is obtained in the same way as for U_{VP} by subtracting the unrenormalized free expression from Eq. (28). Carrying out the trace operation as well as the angular part of the k integration and employing once more the spherical wave decomposition, Eq. (62), this leads to

$$\Delta E^{\mathrm{WK}}_{\mathrm{VP,pot}} = -\frac{e^2}{\pi^2}\sum_{l=0}^{\infty}(2l+1)\int_0^\infty dk\langle a_n|\alpha^\mu j_l(kx)\mathbf{C}^l(\hat{\mathbf{x}})|a_n\rangle\left\{\sum_{\substack{q\\E_q>0}}\sum_{\substack{r\\E_r<0}}\frac{\langle\Phi_q|\alpha_\mu j_l(ky)\mathbf{C}^l(\hat{\mathbf{y}})|\Phi_r\rangle\langle\Phi_r|e\boldsymbol{\alpha}\cdot\mathbf{A}|\Phi_q\rangle}{E_q-E_r}\right.$$

$$\left.-\sum_{\substack{s\\E_s>0}}\sum_{\substack{t\\E_t<0}}\frac{\langle\varphi_s|\alpha_\mu j_l(ky)\mathbf{C}^l(\hat{\mathbf{y}})|\varphi_t\rangle\langle\varphi_t|e\boldsymbol{\alpha}\cdot\mathbf{A}|\varphi_s\rangle}{E_s-E_t}\right\}. \tag{92}$$

Within the loop, the sums are again restricted to electron or positron states, respectively. In the partial wave decomposition evaluation in κ, the vectors of α matrices present allow the coupling between states of different κ, in particular, $\kappa_r=-\kappa_q-1,\kappa_q,-\kappa_q+1=:\tilde{\kappa}_{-1},\tilde{\kappa}_0,\tilde{\kappa}_1$, and accordingly for s and t. Furthermore, the term $\mu=0$ does not contribute due to the angular integrations which is also clear from intuitive reasoning. A simple vacuum polarization interaction is not expected to change a vectorlike interaction into one with a scalar component. The final expression of the partial wave expansion of $\Delta E^{\mathrm{WK}}_{\mathrm{VP,pot}}$ then reads

$$\Delta E^{\mathrm{WK}}_{\mathrm{VP,pot}} = -\frac{e^2}{\pi^2}\sum_{\kappa=\pm1}^{\infty}\sum_{\kappa'=\tilde{\kappa}_{-1}}^{\tilde{\kappa}_1}\sum_{l=0}^{\infty}(2l+1)\int_0^\infty dk\langle a_n|\alpha^\mu j_l(kx)\mathbf{C}^l(\hat{\mathbf{x}})|a_n\rangle$$

$$\times\left\{\sum_{\substack{q\\E_q>0}}\sum_{\substack{r\\E_r<0}}\frac{\langle\Phi_{q,\kappa}|\alpha_\mu j_l(ky)\mathbf{C}^l(\hat{\mathbf{y}})|\Phi_{r,\kappa'}\rangle\langle\Phi_{r,\kappa'}|e\boldsymbol{\alpha}\cdot\mathbf{A}|\Phi_{q,\kappa}\rangle}{E_{q,\kappa}-E_{r,\kappa'}}\right.$$

$$\left.-\sum_{\substack{s\\E_s>0}}\sum_{\substack{t\\E_t<0}}\frac{\langle\varphi_{s,\kappa}|\alpha_\mu j_l(ky)\mathbf{C}^l(\hat{\mathbf{y}})|\varphi_{t,\kappa'}\rangle\langle\varphi_{t,\kappa'}|e\boldsymbol{\alpha}\cdot\mathbf{A}|\varphi_{s,\kappa}\rangle}{E_s-E_t}\right\}, \tag{93}$$

where the summations over the angular quantum numbers κ are specified explicitly. From the l summation, only $l=1$ contributes due to the angular momentum summation rules, and the final expression reads

$$\Delta E^{\mathrm{WK}}_{\mathrm{VP,pot}} = \frac{e^2}{\pi^2}\left(\frac{eB_z}{2}\right)\sum_{\kappa=\pm1}^{\infty}\sum_{\kappa'=\tilde{\kappa}_{-1}}^{\tilde{\kappa}_1}3\int dk\,\mathcal{Q}[(n,\kappa_{a_n}),(n,\kappa_{a_n});k,l=1]$$

$$\times\left\{\sum_{\substack{q\\E_q>0}}\sum_{\substack{r\\E_r<0}}\frac{\mathcal{R}[(r,\kappa'),(q,\kappa)]}{E_{q,\kappa}-E_{r,\kappa'}}\{\mathcal{A}^1_{\mathrm{VP}}(\kappa_{a_n},\kappa,\kappa';l=l)\,\mathcal{Q}[(r,\kappa'),(q,\kappa);k,l=1]\right.$$

$$+\mathcal{A}^2_{\mathrm{VP}}(\kappa_{a_n},\kappa,\kappa';l=1)\,\mathcal{Q}[(q,\kappa),(r,\kappa');k,l=1]+\mathcal{A}^3_{\mathrm{VP}}(\kappa_{a_n},\kappa,\kappa';l=1)\,\mathcal{Q}[(q,\kappa),(r,\kappa');k,l=1]$$

$$+\mathcal{A}^4_{\mathrm{VP}}(\kappa_{a_n},\kappa,\kappa';l=1)\,\mathcal{Q}[(r,\kappa'),(q,\kappa);k,l=1]\}$$

$$-\sum_{\substack{s\\E_s>0}}\sum_{\substack{t\\E_t<0}}\frac{\mathcal{R}[(s,\kappa'),(t,\kappa)]}{E_s-E_t}\{\mathcal{A}^1_{\mathrm{VP}}(\kappa_{a_n},\kappa,\kappa';l=1)\,\mathcal{Q}[(t,\kappa'),(s,\kappa);k,l=1]$$

$$+\mathcal{A}^2_{\mathrm{VP}}(\kappa_{a_n},\kappa,\kappa';l=1)\,\mathcal{Q}[(s,\kappa),(t,\kappa');k,l=1]+\mathcal{A}^3_{\mathrm{VP}}(\kappa_{a_n},\kappa,\kappa';l=1)\,\mathcal{Q}[(s,\kappa),(t,\kappa');k,l=1]$$

$$\left.+\mathcal{A}^4_{\mathrm{VP}}(\kappa_{a_n},\kappa,\kappa';l=1)\,\mathcal{Q}[(t,\kappa'),(s,\kappa);k,l=1]\}\right\} \tag{94}$$

The angular factors are given in Appendix B and the radial integrals $\mathcal{Q}$ and $\mathcal{R}$ are defined in Appendix C. The further evaluation of all radial integrals is carried out in the same manner as in all other cases. Again, values of $|\kappa|\leqslant 30$ are numerically meaningful for almost all except very low Z. For $Z\leqslant 20$, however, the convergence becomes very poor. Higher $|\kappa|$ are prevented by the numerical accuracy of our present code, and for $Z\leqslant 10$ almost no meaningful value is obtained at all. However, contrary to the vertex contribution mentioned above, the total $\Delta E_{\mathrm{VP,pot}}$ contribution is rather small for low Z and thus the total precision of our calculations is hardly influenced by this drawback. We will point out this problem once more in Sec. V.

IV. OTHER CONTRIBUTIONS

Up to now, we have dealt mainly with the QED contributions of order α/π which form the major topic of this work.

There are several other contributions beyond the relativistic spin-orbit interaction which have to be discussed, at least briefly. These comprise nuclear size, shape, mass, internal structure, and also QED effects of higher order.

A. Nuclear properties

The finite nuclear size leads to a deviation from the analytically derived formula (7) for the g_J factor of a bound electron even without considering other effects. The binding potential is slightly altered due to the extended charge distribution within the nucleus. The size of the nucleus is commonly specified by

$$r_{\rm rms}=\langle r^2\rangle^{1/2}=\left(\int dr r^4\rho(r)\Big/\int dr r^2\rho(r)\right)^{1/2}, \quad (95)$$

where $\rho(r)$ is the charge distribution of a spherically symmetric nucleus. From Lamb shift investigations it is known that not only the size of the nucleus has an effect but also its shape [101] which demands a realistic description of the nuclear charge distribution. We employed the two-parameter Fermi distribution for evaluating the finite size correction to g_j given by Eq. (7), which reads

$$Ze\rho_{2p\rm Fermi}(r)=Ze\frac{N}{1+e^{(r-c)/a}}. \quad (96)$$

The index ''$2p$'' denotes ''two-parameter'' (a and c), where c is the half-density radius and a is a measure for the skin thickness, related to $t=4\ln 3a$. t indicates the radial distance over which the charge density falls from 90 to 10 % of its value at $r=0$. N is a properly chosen normalization constant. To a good approximation [102],

$$c^2=\frac{5}{3}r_{\rm rms}^2-\frac{7}{3}a^2\pi^2 \quad (97)$$

and

$$N=\frac{3}{4\pi c^3}\left(1+\frac{\pi^2a^2}{c^2}\right)^{-1} \quad (98)$$

hold. Further details are given, e.g., by Ref. [103].

In strong-field QED calculations it can be seen that the effect of nuclear size depends mainly on the radius chosen and only little on the actual model employed [101,104]. An exception is hydrogenlike systems with $Z>100$ [101]. In this case higher moments of the charge distribution have to be considered at least approximatively, see, for instance, the evaluations performed by Shabaev [102]. For the present investigation these considerations are not necessary and the QED calculations are thus carried out employing a reasonable but easy to handle charge distribution such as the homogeneously charged ball as is utilized in the present study.

Another effect of interest, in particular for lighter ions, is the finite nuclear mass. In calculations of strong-field QED the electromagnetic potential of the nucleus is normally considered as time independent and external, thus referring to either an infinitely heavy nucleus or to a proper separation into center-of-mass and relative coordinates. Even the latter, however, yields a value of the finite nuclear-mass correction wrong by more than 50% in Lamb shift calculations on the the lowest lying states in heavy hydrogenlike ions [105,106]. An equally simple estimate for the g factor can thus not be expected to yield a higher accuracy. However, up to now there is a lack of calculations beyond expansions in α, $Z\alpha$, and the mass-ratio electron-nucleus m_e/M_N. These expansions were obtained in 1970 independently by Grotch [38,39] utilizing an expansion of the corresponding two-particle Dirac equation, and also by Faustov [41], who employed an effective potential method. Their results were reproduced by Close and Osborn [42] starting from a group theoretical approach.

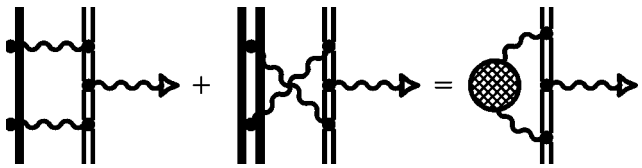

FIG. 5. Nuclear polarization correction to the g_j factor in terms of Feynman diagrams. The heavy double line represents the nucleus. The nuclear polarization can be envisaged as a modified self-energy.

The recoil contribution known so far reads

$$g_{j\ \rm recoil}=(Z\alpha)^2\left[\left(\frac{m_e}{M_N}\right)-(1+Z)\left(\frac{m_e}{M_N}\right)^2\right]+(Z\alpha)^2\left(\frac{\alpha}{\pi}\right)\left[-\frac{1}{3}\left(\frac{m_e}{M_N}\right)+\frac{3-2Z}{6}\left(\frac{m_e}{M_N}\right)^2\right]. \quad (99)$$

This equation is exact to orders $(Z\alpha)^2$, (α/π), and $(m_e/M_N)^2$. The last two expansions are reasonable also for high-Z systems. For these systems, the expansion into powers of $(Z\alpha)$ can only be considered as an approximation which serves as an order-of-magnitude estimate.

Another feature of the nucleus is its internal structure. The nucleus can be envisaged as consisting of protons and neutrons which in turn are formed by quarks and gluons. This composite object can undergo a virtual excitation and deexictation exchanging two photons with the propagating electron as depicted in Fig. 5. The nuclear polarization plays an important role in muonic systems due to the large overlap of the muonic wave function with the nucleus and, in addition, also because the transition energies in a muonic atom are of similar size as the excitation energies of the nucleus [100].

In electronic systems, evaluations of the nuclear polarization effect have been carried out only as corrections to the QED Lamb shift predictions for the lowest-lying states of heavy few-electron ions [1,107–110]. Here a technique was developed to envisage the whole process as an additional effective self-energy interaction by inserting a nuclear polarization function into the photon propagator present in the self-energy operator, Eq. (23) [111,112]. For heavy nuclei, the calculation yields an order-of-magnitude value of the

same size as the QED corrections of order α^2, or even less in $^{208}Pb^{81+}$ where several nuclear polarization contributions can be shown to nearly cancel [109]. However, due to the uncertainty of nuclear parameters and also due to the restriction to the lowest lying excitations in all calculations carried out so far, the nuclear polarization correction is supposed to have an error margin of up to 50% of its value, thus restricting the precision of the whole Lamb shift prediction.

For the QED corrections to the Zeeman effect under consideration here, nuclear polarization calculations were not yet carried out. Their result is not expected to be larger than the bound-state QED contributions of order $(\alpha/\pi)^2$ and also to have an influence on the total prediction value of even less than that in Lamb shift calculations [113]. Their calculation becomes more urgent as soon as there are complete calculations of all QED effects of order $(\alpha/\pi)^2$ to the g factor, at least for obtaining an order-of-magnitude estimate. At present, we are going to neglect completely any nuclear polarization contribution in our further discussions.

B. QED effects of higher orders

The main goal of this work was to perform a complete calculation of the QED binding effects of order α/π, corresponding to one internal photon line in the corresponding diagrams in Fig 2. However, the sum of these diagrams forms only the second coefficient in the expansion

$$g_{j1s_{1/2}}(Z)=2\left[C^{(0)}+C^{(2)}\left(\frac{\alpha}{\pi}\right)+C^{(4)}\left(\frac{\alpha}{\pi}\right)^2+C^{(6)}\left(\frac{\alpha}{\pi}\right)^3+C^{(8)}\left(\frac{\alpha}{\pi}\right)^4+\cdots\right], \tag{100}$$

where $C^{(0)}$ contains the Dirac g factor of the free electron as well as the relativistic spin orbit coupling contribution, Eq. (7), due to binding and does not comprise any quantum electrodynamical correction. It is given by

$$C^{(0)}=\tfrac{1}{3}\left[1+2\sqrt{1-(Z\alpha)^2}\right]. \tag{101}$$

The notation adopted here is that of Refs. [50] and [114], where QED corrections to the free electron g factor are denoted by

$$g_{\text{free}}=2\left[1+A_1^{(2)}\left(\frac{\alpha}{\pi}\right)+A_1^{(4)}\left(\frac{\alpha}{\pi}\right)^2+A_1^{(6)}\left(\frac{\alpha}{\pi}\right)^3+A_1^{(8)}\left(\frac{\alpha}{\pi}\right)^4+\cdots\right]. \tag{102}$$

The A_1 refer to diagrams with only electron lines present [114], i.e., no muonic and tauonic lines and no strong and weak interactions. The coefficients read

$$A_1^{(2)}=\frac{1}{2}\quad\text{(Refs. [26,27])},$$

$$A_1^{(4)}=\frac{197}{144}+\left(\frac{1}{2}-3\ln 2\right)\zeta(2)+\frac{3}{4}\zeta(3)=-0.328\,478\,965\ldots\quad\text{(Refs. [31,32])},$$

$$A_1^{(6)}=\frac{83}{72}\pi^2\zeta(3)-\frac{215}{24}\zeta(5)+\frac{100}{3}\left[\left(a_4+\frac{1}{24}\ln^4 2\right)-\frac{1}{24}\pi^2\ln^2 2\right]-\frac{239}{2160}\pi^4+\frac{139}{18}\zeta(3)-\frac{298}{9}\pi^2\ln 2+\frac{17101}{810}\pi^2+\frac{28259}{5184}=1.181\,241\,456\cdots\quad\text{(Ref. [33])},$$

$$A_1^{(8)}=-1.509\,8\,(384)\quad\text{(Ref. [34])}, \tag{103}$$

where $\zeta(k)=\Sigma_{n=1}^{\infty}(1/n^k)$ and $a_4=\Sigma_{n=1}^{\infty}[1/(2^n n^4)]$. As already mentioned, $A_1^{(8)}$ represents 891 Feynman diagrams. Their analytical evaluation with modern algebraic computer programs has just begun, and the error specified by Hughes and Kinoshita is a rather conservative error margin of the numerical calculations carried out so far, according to the authors.

Additional contributions to the g factor of a free electron result from nonelectronic QED contributions, in particular vacuum polarization loops containing muons and tauons, which contribute 5.442×10^{-12}; vacuum polarization loops containing hadronic particles, contributing $3.284(54)\times10^{-12}$; and weak interaction effects at a level of 6×10^{-14} [34] within the standard model.

From these representations it is clear that each $C^{(2i)}$ can be written as

$$C^{(2i)}=A_1^{(2i)}+\text{QED binding effects}. \tag{104}$$

Expanding the QED binding effects into a power series of $(Z\alpha)$ yields the expression obtained by Grotch as the leading term

$$C^{(2)}(Z)=\frac{1}{2}+\frac{(Z\alpha)^2}{12}+\cdots. \tag{105}$$

In Fig. 6 we display the QED corrections of order $(\alpha/\pi)^2$. These or corrections of even higher order have not yet been calculated considering bound state QED. To have a reasonable starting point for this, at least all QED corrections of order α^2 to the Lamb shift should be known properly, a task which is still pending [1,115]. An estimate for the total order of magnitude of this correction can be obtained by observing that all coefficients $A_1^{(2i)}$ in Eq. (103) are of magnitude 1.

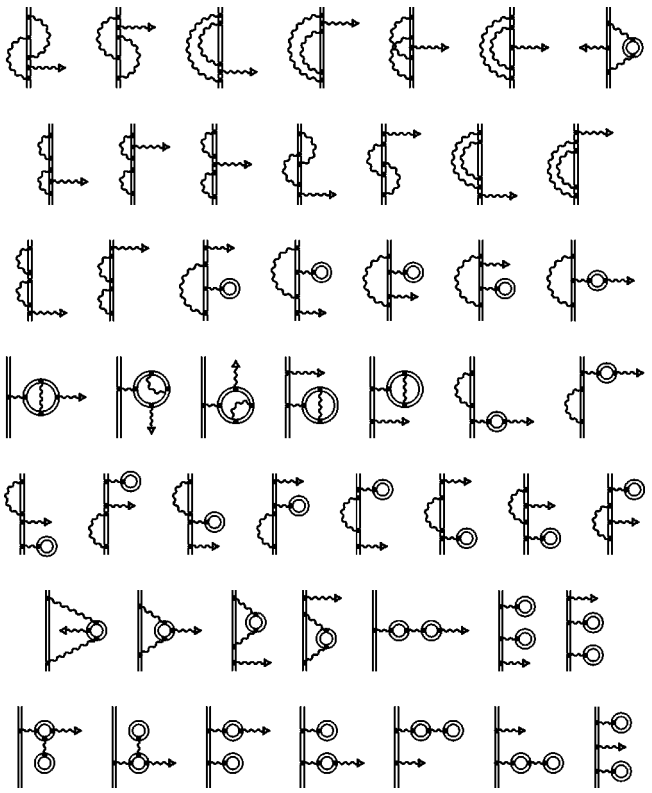

FIG. 6. QED diagrams of order $(\alpha/\pi)^2$ to g_j. Only the first row of diagrams has to be considered for the g factor of the free electron.

Therefore it is reasonable to assume a scaling by a factor (α/π) also for the bound state contributions, and an estimate reads

$$\text{QED binding effects, order } (\alpha/\pi)^2 = \left(\frac{\alpha}{\pi}\right) \times [\text{QED binding effects, order } (\alpha/\pi)]. \tag{106}$$

Without any full calculation of all diagrams of order $(\alpha/\pi)^2$, no theoretical value for $g_{j1s_{1/2}}$ can claim an accuracy better than at least three times the above estimate of the $(\alpha/\pi)^2$ contributions.

V. RESULTS

The results of our calculations are presented in detail in Tables I–III for some Z. A summary for all Z under investigation is given in Table IV. The grid of Z we chose is quite tight throughout the whole range from $Z=1$ to $Z=94$, including nearly all even Z (except the unstable Po) and in addition also all odd $Z<18$ as well as those where hyperfine structure measurements in hydrogenlike systems were carried out and also a few more to tighten the calculation around the heaviest stable odd-Z nuclei. When comparing a high precision experiment with theory, any interpolation of a sparsely given theoretical grid is rather meaningless. For this reason we present a comprehensive tabulation of values.

As pointed out, all calculations were carried out in the Feynman gauge employing the renormalization procedures mentioned above. The error margins specified are purely numerical resulting from the integrations over the photon momentum k and the partial-wave extrapolation over l or $|\kappa|$, respectively. Error propagation is always carried out by linearly adding the errors in order not to underestimate any overlooked systematic numerical effect.

The self-energy contributions have also been calculated by Blundell *et al.* for a number of Z employing a point nucleus [50]. We include their values in our Tables I and II for comparison after multiplying them accordingly by $(2\alpha/\pi)$, as they were specified in terms of $C^2(Z\alpha)$ in Ref. [50]. In that work, only up to six significant figures were displayed.

Table I displays all contributions to $g_{j\mathrm{SE,WF,irred}}$ for a few Z, calculated by utilizing Eqs. (56), (59), and (65). The numerical error resulting from the terms with zero and one nuclear-potential interaction is rather small for low Z and empirically even an anticorrelation between the behavior of both terms is observed, if the number of grid points in the p integration is altered. Therefore, the error margin of both terms is combined. The remaining term, $g^{[\geqslant 2]}_{j\mathrm{SE,WF,irred}}$, is calculated employing a partial wave expansion up to $l=30$. The numerical accuracy is in most cases already sufficient employing partial waves up to $l=20$.

The contributions to $g_{j\mathrm{SE,ve}}+g_{j\mathrm{SE,WF,red}}$ are given in Table II for some Z, where the results of Eqs. (70), (69), and (76) and (79) are displayed. For $Z\leqslant 20$, the separate calculation of $g^{[1]}_{j\mathrm{SE,WF,red}}+g^{[1]}_{j\mathrm{SE,ve}}$ according to Eqs. (81) and (82) is also presented. In these separate calculations, pointlike nuclei were employed as discussed above, due to the smallness of any finite-size effect on QED corrections in this range of Z. For calcium and carbon, calculations of $g^{[\geqslant 1]}_{j\mathrm{SE,WF,red}}+g^{[\geqslant 1]}_{j\mathrm{SE,ve}}$ are also shown. If pointlike nuclei are considered, the calculation from $g^{[\geqslant 1]}_{j\mathrm{SE,WF,red}}+g^{[\geqslant 1]}_{j\mathrm{SE,ve}}$ agrees well within its error margins with the split calculation for Ca. However, for extended nuclei a small discrepancy shows up which necessitates the scheme of Eqs. (76) and (79) for $Z\geqslant 20$. For carbon, Eqs. (76) and (79) yield the same result for both pointlike and extended nuclei. It does not agree with the corresponding one from the split calculation which is obviously due to a failure in extrapolating Eqs. (76) and (79) to higher partial waves. For carbon, the partial wave contribution changes sign around $l=12$, which is also indicated by Fig. 7. Therefore, our separate treatment of the $g^{[1]}_{j\mathrm{SE,WF,red}}+g^{[1]}_{j\mathrm{SE,ve}}$ terms is well justified and improves the theoretical prediction also in the Z range under current experimental investigation. Figure 7 displays the behavior of the partial waves of $g^{[\geqslant 1]}_{j\mathrm{SE,WF,red}}+g^{[\geqslant 1]}_{j\mathrm{SE,ve}}$ over the whole Z range. The term for $l=0$ is not shown. For U, Ba, and Ca all terms except the first are <0, but for Ca the whole contribution is >0. For C, in addition to the sign change, numerical instability becomes visible for higher l, making a proper extrapolation for $l>20$ impossible.

In general, our values agree within 10^{-6} with those presented by Blundell *et al.* for pointlike nuclei. A closer agreeement cannot be expected due to the number of figures

TABLE I. The different contributions to $g_{j\mathrm{SE,WF,irred}}$ in Feynman gauge. All values are absolute contributions to g_j ($1/\alpha = 137.035\,989\,5$) and displayed in units of 10^{-6}. For $g^{[0]}_{j\mathrm{SE,WF,irred}}$ and $g^{[1]}_{j\mathrm{SE,WF,irred}}$, an uncertainty is specified for the sum only. Note, that all the values presented here are strictly gauge dependent. Only the total result (last column) is meaningful also beyond our calculations. The results obtained by Blundell *et al.* [50] are shown for comparison. For $Z=90$, the result of a point-nucleus calculation is also shown (90●).

Z	$g^{[0]}_{j\mathrm{SE,WF,irred}}$	$g^{[1]}_{j\mathrm{SE,WF,irred}}$	$\Delta(g^{[0]}_{j\mathrm{SE,WF,irred}} + g^{[1]}_{j\mathrm{SE,WF,irred}})$	$g^{[\geq 2]}_{j\mathrm{SE,WF,irred}}$	$g_{j\mathrm{SE,wf,irred.}}$
1	1.0814	0.3092	(0.0001)	0.1386(3)	1.5292(4)
5	20.2403	1.5513	(0.0001)	3.3158(3)	25.1075(4)
				(Blundell *et al.* :	25.13)
6	27.9866	1.3714	(0.0001)	4.7067(3)	34.0647(4)
10	68.3632	−1.8975	(0.0001)	12.2777(3)	78.7434(4)
				(Blundell *et al.* :	78.74)
15	135.8677	−11.0525	(0.0001)	25.4194(3)	150.2346(4)
				(Blundell *et al.* :	150.24)
18	183.3569	−18.4170	(0.0001)	34.8236(3)	199.7635(4)
20	217.3241	−23.7578	(0.0002)	41.607(1)	235.174(1)
				(Blundell *et al.* :	235.26)
30	405.9092	−49.0996	(0.0002)	80.375(1)	437.5185(1)
				(Blundell *et al.* :	437.39)
40	607.4052	−56.7027	(0.0005)	125.836(1)	676.538(2)
				(Blundell *et al.* :	676.64)
50	800.1046	−26.0449	(0.0005)	178.604(1)	952.664(2)
				(Blundell *et al.* :	952.03)
56	902.9506	19.5921	(0.0005)	214.973(2)	1137.516(3)
60	963.3081	64.5562	(0.0005)	241.798(2)	1269.662(3)
				(Blundell *et al.* :	1270.44)
67	1047.8501	177.2739	(0.0005)	295.023(3)	1520.147(3)
70	1073.9206	241.1482	(0.001)	320.827(3)	1635.896(4)
				(Blundell *et al.* :	1638.10)
75	1100.507	372.431	(0.005)	368.755(4)	1841.693(9)
80	1101.872	539.654	(0.005)	423.970(5)	2065.50(1)
				(Blundell *et al.* :	2072.61)
81	1098.608	578.046	(0.005)	436.033(5)	2112.69(1)
82	1094.053	618.216	(0.005)	448.465(5)	2160.73(1)
83	1088.158	660.218	(0.005)	461.278(5)	2209.65(1)
90	1004.017	1012.081	(0.005)	563.071(8)	2579.17(1)
				(Blundell *et al.* :	2601.93)
90●	985.497	1046.324	(0.005)	569.407(10)	2601.23(2)
92	963.951	1133.981	(0.005)	596.628(8)	2694.56(1)
94	914.862	1268.134	(0.005)	632.756(8)	2815.75(1)

presented in that work. In the high-Z range, stronger deviations are observed in particular for the $g_{j\mathrm{SE,WF,irred}}$ contribution. This is most probably due to nuclear size effects. We could reproduce Blundell's values pretty well by setting $r_{\mathrm{rms}}(^{232}_{90}\mathrm{Th}) = 0$, as indicated in Tables I and II. This yields also an estimate of the nuclear size effect on the QED contributions which can amount to up to 1% of the value in the region of high Z. The finite nuclear size should therefore always be considered in high-precision calculations. On the low Z side, the values obtained in Ref. [50] for $g^{[\geq 1]}_{j\mathrm{SE,WF,red}} + g^{[\geq 1]}_{j\mathrm{SE,ve}}$ also suffer from difficulties in the partial wave expansion, as explicitly stated there, although a different numerical scheme was employed in that work.

Let us now turn to the vacuum polarization contributions $g^{\mathrm{Ueh}}_{j\mathrm{VP,WF}}$ (49), $g^{\mathrm{WK}}_{j\mathrm{VP,WF}}$ (91), and $g^{\mathrm{WK}}_{j\mathrm{VP,pot}}$ (92), which have not been calculated before (apart from our previously reported numbers [51]). The results are presented in Table III for some Z. The dominant contribution is that of $g^{\mathrm{Ueh}}_{j\mathrm{VP,WF}}$ which causes no difficulties in the calculation. The higher order terms to $g_{j\mathrm{VP,WF}}, g^{\mathrm{WK}}_{j\mathrm{VP,WF}}$, are only about 5% of the Uehling value even for U^{91+} which is roughly the same amount as in Lamb-shift calculations [116]. Their expansion in $|\kappa|$ is also performed without problems. A value of $|\kappa| = 15$ is sufficient for almost every Z. Considering higher values of $|\kappa|$ does not

TABLE II. The different contributions to $(g_{jSE,WF,red}+g_{j,SE,ve})$ in Feynman gauge and the calculation schemes as discussed in the text. All values are absolute contributions to g_j $(1/\alpha=137.035\,989\,5)$ and displayed in units of 10^{-6}. The separate $(g^{[1]}_{jSE,WF,red}+g^{[1]}_{jSE,ve})$ calculations for the low-Z region are also shown. For $Z=20$, the results from all calculation schemes are displayed for comparison. For $Z\geqslant 20$, we employ the scheme which allows no separation of the $g_j^{[1]}$ terms but a consideration of extended nuclei. Further discussion can be found in the text. Note, that all the values presented here are strictly gauge dependent. Only the total result (last column) is meaningful also beyond our calculations. Values presented by Blundell *et al.* [50] are displayed in parentheses. For $Z=90$, the result of a point-nucleus calculation is also shown (90●).

Z	$g^{[0]}_{jSE,ve}$	$g^{[0]}_{jSE,WF,red}$	$(g^{[1]}_{jSE,WF,red}+g^{[1]}_{jSE,ve})$	$(g^{[\geqslant 2]}_{jSE,WF,red}+g^{[\geqslant 2]}_{jSE,ve})$	$(g^{[\geqslant 1]}_{jSE,WF,red}+g^{[\geqslant 1]}_{jSE,ve})$	$(g_{jSE,WF,red}+g_{jSE,ve})$
1	−33863.0312(2)	36183.8068(1)	0.5025(1)	0.0331(1)	0.5356(2)	2321.3112(5)
5	−19024.5377(2)	21315.9529(1)	6.1031(1)	0.7670(1)	6.8701(2)	2298.2853(5)
	[−19024.54	21315.96	Blundell *et al.*		6.88(5)]	
6	−17373.1336(2)	19653.8716(1)	7.7945(1)	1.0752(1)	8.8697(2)	2289.6077(5)
			without separation of the $g_j^{[1]}$ terms:		9.05(5)	
10	−12833.3722(2)	15063.1985(1)	14.3478(2)	2.6180(1)	16.9658(3)	2246.7921(6)
	[−12833.35	15063.07	Blundell *et al.*		16.82]	
15	−9380.7864(2)	11535.0738(1)	20.7702(3)	4.7580(5)	25.5282(8)	2179.816(1)
	[−9380.75	11534.98	Blundell *et al.*		25.32(5)]	
18	−7895.6827(2)	10000.9797(1)	23.3407(4)	5.860(1)	29.201(1)	2134.498(2)
20			24.4979(4)	6.417(1)	30.915(1)	
			point nucleus, without separation of the $g_j^{[1]}$ terms:		30.92(1)	
	−7062.0775(2)	9133.7931(1)		extended nucleus:	30.97(1)	2102.69(1)
	[−7062.07	9133.70	Blundell *et al.*		30.61]	
30	−4068.0521(2)	5967.4785(1)			29.98(1)	1929.40(1)
	[−4068.04	5967.46	Blundell *et al.*		29.96]	
40	−2207.8932(2)	3937.4706(2)			13.27(1)	1742.85(1)
	[−2207.84	3937.37	Blundell *et al.*		13.29]	
50	−958.1935(4)	2527.6059(4)			−17.249(5)	1552.163(6)
	[−958.07	2527.38	Blundell *et al.*		−17.24]	
56	−398.6146(5)	1878.1174(5)			−40.836(5)	1438.667(6)
60	−85.1609(4)	1507.5978(5)			−58.204(5)	1364.233(6)
	[−84.83	1507.14	Blundell *et al.*		−58.21]	
67	370.2726(3)	958.1696(3)			−90.687(5)	1237.756(6)
70	534.5147(3)	756.0130(3)			−105.032(5)	1185.496(6)
	[535.08	755.20	Blundell *et al.*		−104.99]	
75	773.0151(2)	457.5732(3)			−128.876(5)	1101.712(6)
80	972.5097(2)	202.3266(3)			−151.873(5)	1022.963(6)
	[973.35	201.06	Blundell *et al.*		−151.68]	
81	1008.1688(2)	156.0287(3)			−156.287(5)	1007.911(6)
82	1042.4930(2)	111.2394(3)			−160.617(5)	993.115(6)
83	1075.5125(2)	67.9298(2)			−164.857(5)	978.585(5)
90	1272.4811(2)	−196.0925(2)			−191.212(5)	885.177(5)
	[1273.60	−197.81	Blundell *et al.*		−190.42]	
90●	1273.6053(2)	−197.8180(1)			−190.460(5)	885.327(5)
92	1318.5106(2)	−259.6528(1)			−197.373(5)	861.485(5)
94	1360.3190(2)	−318.2716(1)			−202.719(5)	839.328(5)

change the value of Eq. (91) within the error margins. Only for very low Z, do numerical instabilities cause minor problems. However, these problems occur only for total contributions of $g^{WK}_{jVP,WF}<10^{-11}$ where the whole contribution itself is negligible. To obtain an estimate for the finite nuclear size effects on the vacuum polarization calculations as well, we have also carried them out for Th, employing a point nucleus. The values are given in Table III and indicate a difference at the 10^{-5} level for the vacuum polarization contributions, thus again showing the need for considering the size of the nucleus properly.

Problems occur when evaluating the potential correction for small Z, $g^{WK}_{jVP,pot}$, Eq. (92). The convergence according to $\pm\kappa$ is displayed in Fig. 8 for a number of Z. As can be seen,

TABLE III. The vacuum polarization contributions of order α/π to the g_j factor of an electron bound in a hydrogenlike ion. All values are absolute contributions to g_j $(1/\alpha = 137.035\,989\,5)$. The last column indicates their total sum, except for H and He^+, where it is meaningless due to the large error in $g_{j\mathrm{VP,pot}}$. For $Z=90$, the result of a point-nucleus calculation is also shown (90●).

Z	$g^{\mathrm{Ueh}}_{j\mathrm{VP,WF}}$	$g^{\mathrm{WK}}_{j\mathrm{VP,WF}}$	$g_{j\mathrm{VP,WF}}$	$g_{j\mathrm{VP,pot}}$	$g_{j\mathrm{VP,\,tot}}$
1	$-6.944(5)\times10^{-12}$	$0.7(2)\times10^{-16}$	$-6.944(5)\times10^{-12}$	$0.0(3)\times10^{-9}$	
2	$-1.09898(2)\times10^{-10}$	$0.5(1)\times10^{-14}$	$-1.09893(3)\times10^{-10}$	$0.0(3)\times10^{-9}$	
3	$-5.50494(3)\times10^{-10}$	$5.4(1)\times10^{-14}$	$-5.50440(4)\times10^{-10}$	$0.0(3)\times10^{-9}$	$-5.5(3.0)\times10^{-10}$
4	$-1.72222(1)\times10^{-9}$	$2.99(3)\times10^{-13}$	$-1.72192(1)\times10^{-9}$	$0.0(3)\times10^{-9}$	$-1.7(3)\times10^{-9}$
5	$-4.16369(1)\times10^{-9}$	$1.11(1)\times10^{-12}$	$-4.16258(2)\times10^{-9}$	$0.0(3)\times10^{-9}$	$-4.2(3)\times10^{-9}$
6	$-8.55285(1)\times10^{-9}$	$3.28(1)\times10^{-12}$	$-8.54957(2)\times10^{-9}$	$0.0(3)\times10^{-9}$	$-8.5(3)\times10^{-9}$
10	$-6.37640(1)\times10^{-8}$	$6.506(2)\times10^{-11}$	$-6.36989(1)\times10^{-8}$	$0.0(3)\times10^{-9}$	$-6.37(3)\times10^{-8}$
15	$-3.11298(1)\times10^{-7}$	$6.8385(3)\times10^{-10}$	$-3.10614(1)\times10^{-7}$	$0.21(10)\times10^{-8}$	$-3.09(1)\times10^{-7}$
18	$-6.33616(1)\times10^{-7}$	$1.9539(2)\times10^{-9}$	$-6.31662(1)\times10^{-7}$	$0.6(2)\times10^{-8}$	$-6.26(2)\times10^{-7}$
20	$-9.55031(5)\times10^{-7}$	$3.5769(3)\times10^{-9}$	$-9.51454(5)\times10^{-7}$	$1.0(3)\times10^{-8}$	$-9.41(3)\times10^{-7}$
30	$-4.63685(1)\times10^{-6}$	$3.6139(1)\times10^{-8}$	$-4.60071(1)\times10^{-6}$	$1.01(2)\times10^{-7}$	$-4.499(2)\times10^{-6}$
40	$-1.43630(1)\times10^{-5}$	$1.8501(1)\times10^{-7}$	$-1.41780(1)\times10^{-5}$	$4.10(2)\times10^{-7}$	$-1.3768(2)\times10^{-5}$
50	$-3.50887(2)\times10^{-5}$	$6.5837(3)\times10^{-7}$	$-3.44303(2)\times10^{-5}$	$1.225(4)\times10^{-6}$	$-3.3206(4)\times10^{-5}$
56	$-5.57919(3)\times10^{-5}$	$1.26030(1)\times10^{-6}$	$-5.45316(4)\times10^{-5}$	$2.115(4)\times10^{-6}$	$-5.2416(4)\times10^{-5}$
60	$-7.43603(5)\times10^{-5}$	$1.8772(2)\times10^{-6}$	$-7.24831(7)\times10^{-5}$	$2.950(5)\times10^{-6}$	$-6.9534(6)\times10^{-5}$
67	$-1.18898(1)\times10^{-4}$	$3.5673(2)\times10^{-6}$	$-1.15331(1)\times10^{-4}$	$5.007(6)\times10^{-6}$	$-1.10324(7)\times10^{-4}$
70	$-1.43865(1)\times10^{-4}$	$4.6158(2)\times10^{-6}$	$-1.39249(1)\times10^{-4}$	$6.203(6)\times10^{-6}$	$-1.33047(7)\times10^{-4}$
75	$-1.95553(1)\times10^{-4}$	$6.9659(3)\times10^{-6}$	$-1.88587(1)\times10^{-4}$	$8.665(8)\times10^{-6}$	$-1.79922(9)\times10^{-4}$
80	$-2.62673(1)\times10^{-4}$	$1.0286(1)\times10^{-5}$	$-2.52387(2)\times10^{-4}$	$1.186(1)\times10^{-5}$	$-2.4053(1)\times10^{-4}$
81	$-2.78328(1)\times10^{-4}$	$1.1097(1)\times10^{-5}$	$-2.67231(2)\times10^{-4}$	$1.260(1)\times10^{-5}$	$-2.5464(1)\times10^{-4}$
82	$-2.94805(1)\times10^{-4}$	$1.1963(1)\times10^{-5}$	$-2.82842(2)\times10^{-4}$	$1.337(1)\times10^{-5}$	$-2.6947(1)\times10^{-4}$
83	$-3.12138(1)\times10^{-4}$	$1.2886(1)\times10^{-5}$	$-2.99252(2)\times10^{-4}$	$1.419(1)\times10^{-5}$	$-2.8506(1)\times10^{-4}$
90	$-4.61594(1)\times10^{-4}$	$2.1304(1)\times10^{-5}$	$-4.40290(2)\times10^{-4}$	$2.111(1)\times10^{-5}$	$-4.1919(1)\times10^{-4}$
90●	$-4.84549(1)\times10^{-4}$	$2.3342(1)\times10^{-5}$	$-4.61207(2)\times10^{-4}$	$2.126(1)\times10^{-5}$	$-4.3995(1)\times10^{-4}$
92	$-5.15122(1)\times10^{-4}$	$2.4484(1)\times10^{-5}$	$-4.90638(2)\times10^{-4}$	$2.352(1)\times10^{-5}$	$-4.6711(1)\times10^{-4}$
94	$-5.75234(1)\times10^{-4}$	$2.8155(1)\times10^{-5}$	$-5.47079(2)\times10^{-4}$	$2.618(1)\times10^{-5}$	$-5.2090(1)\times10^{-4}$

the contributions change sign twice in the region of low $|\kappa|$, reach a second maximum on the positive side and then slowly tend to decrease again. For medium and high Z, this process takes part within $|\kappa|\leqslant 5$ and the further extrapolation causes no problems. For C^{5+}, however, the second maximum seems to be reached at about $|\kappa|=30$ only, leaving no decreasing tail for carrying out any extrapolation, as $|\kappa|=30$ is also the maximum value of our current calculations, due to numerical stability. Even for Z as large as 30 the numerical instability tends to be as much as 5% of the total value of $g^{\mathrm{WK}}_{j\mathrm{VP,pot}}$. The reason for not improving our calculation at the present stage is the total share of this contribution, which is rather small, compared to $g_{j\mathrm{SE,WF}}$, $g_{j\mathrm{SE,ve}}$, and $g_{j\mathrm{VP,WF}}$. For $Z\leqslant 12$, however, the error of the contribution has to be estimated to be at least 3×10^{-10}, although the actual value might be smaller. This is also indicated by the data points in Fig. 9. All QED contributions calculated so far are displayed in Fig. 9, together with the free QED corrections of orders $(\alpha/\pi)^2$, $(\alpha/\pi)^3$, and $(\alpha/\pi)^4$, Eq. (103).

All QED calculations are summarized in Table IV. By subtracting α/π, the total QED effect of binding is obtained (column 7) which can be compared with the term $(\alpha/\pi)(Z\alpha)^2/6$ [Eq. (105), in column 8] obtained by Grotch [39]. For $Z=1$ and $Z=2$, our calculation agrees with this expansion within the error margins. But already for Li, differences become visible which amount already to 1×10^{-7} for C^{5+}. Both curves are also displayed in Fig. 9. In addition, the total QED binding effect of order (α/π) was multiplied by another factor of (α/π) to obtain the estimate for the binding correction of order $(\alpha/\pi)^2$, as discussed above. This last line indicates the present day limit of theoretical precision for $g_{j1s_{1/2}}$ which cannot be crossed without evaluating 50 additional diagrams. There is no sense in improving the calculation of QED contributions of order α/π which are smaller than this indicated value, and therefore we did not even try to obtain more precise values for $g^{\mathrm{WK}}_{j\mathrm{VP,pot}}$ in the low-Z region. The total numerical uncertainty indicated in column 6 of Table IV is less than the order $(\alpha/\pi)^2$ estimate except for very low Z, and therefore we conclude that our present calculation is sufficient as far as precision is concerned.

Our QED calculation of order α/π is displayed in Table V together with the result of Eq. (7). The nuclear size correction to this contribution is obtained by calculating Eq. (6) with wave functions corresponding to an extended nucleus with r_{rms} as specified. In these calculations, a two-parameter Fermi distribution with $a=0.524$ is employed, except for uranium, where $a=0.5046$ was used, taken from Ref. [117] and thorium ($a=0.511$ from Ref. [118]). The nuclear radii

TABLE IV. The different QED contributions of order α/π to g_j of an electron bound in a hydrogenlike ion, their sum, and the amount due to binding which is obtained after subtracting the term (α/π) of the free electron's g factor. All values are absolute contributions to g_j $(1/\alpha = 137.035\,989\,5)$ and displayed in units of 10^{-6}. The binding correction obtained from the $Z\alpha$ expansion due to Grotch [37] is presented in the last line for comparison. Numerical uncertainties are indicated in parentheses. No given uncertainty indicates an error smaller than one digit of the last displayed figure. The uncertainty of the binding effect (not specified) is always the same as that of the corresponding total QED contribution of order α/π. For $Z \leqslant 14$, the last figure was not rounded off in the binding-effect column.

Z	$g_{j,\mathrm{SE}}$ ve + WF, red	$g_{j,\mathrm{SE}}$ WF, irred	$g_{j,\mathrm{VP}}$ WF	$g_{j,\mathrm{VP}}$ pot	Tot. $g_{j,\mathrm{QED}}$ (order α/π)	Effect of binding (total)	Effect of binding ($Z\alpha$ exp)
1	2321.3112(5)	1.5292(4)	−0.0000	0.0000(3)	2322.840(1)	0.0208	0.0206
2	2317.6975(5)	5.2065(4)	−0.0001	0.0000(3)	2322.904(1)	0.0842	0.0825
3	2312.4908(5)	10.5232(4)	−0.0006	0.0000(3)	2323.013(1)	0.1938	0.1855
4	2305.9589(5)	17.2162(4)	−0.0017	0.0000(3)	2323.173(1)	0.3537	0.3298
5	2298.2853(5)	25.1075(4)	−0.0042	0.0000(3)	2323.389(1)	0.5690	0.5154
6	2289.6077(5)	34.0647(4)	−0.0085	0.0000(3)	2323.664(1)	0.8442	0.7422
7	2280.0359(5)	43.9840(4)	−0.0157	0.0000(3)	2324.004(1)	1.1846	1.0102
8	2269.6606(6)	54.7815(4)	−0.0265	0.0000(3)	2324.416(1)	1.5959	1.3194
9	2258.5579(6)	66.3875(4)	−0.0421	0.0000(3)	2324.903(1)	2.0836	1.6699
10	2246.7921(6)	78.7434(4)	−0.0637	0.0000(3)	2325.472(1)	2.6522	2.0616
11	2234.4236(7)	91.7989(4)	−0.0925	0.0003(3)	2326.130(1)	3.3106	2.4945
12	2221.4992(8)	105.5111(4)	−0.1300	0.0004(4)	2326.881(2)	4.0610	2.9686
13	2208.0640(8)	119.8424(4)	−0.1777	0.0008(5)	2327.729(2)	4.9098	3.4840
14	2194.1583(9)	134.7596(4)	−0.2374	0.0014(10)	2328.682(2)	5.8623	4.0406
15	2179.816(1)	150.2346(4)	−0.3106	0.002(1)	2329.742(3)	6.922	4.639
16	2165.075(1)	166.2416(4)	−0.3994	0.003(1)	2330.920(3)	8.101	5.278
17	2149.959(1)	182.7576(4)	−0.5057	0.005(2)	2332.216(3)	9.396	5.958
18	2134.498(2)	199.7635(4)	−0.6317	0.006(2)	2333.636(4)	10.816	6.679
20	2102.69(1)	235.174(1)	−0.9515	0.010(3)	2336.92(1)	14.10	8.25
22	2069.63(1)	272.355(1)	−1.3779	0.018(3)	2340.62(1)	17.80	9.98
24	2035.71(1)	311.212(1)	−1.9321	0.033(3)	2345.02(1)	22.21	11.87
26	2000.95(1)	351.672(1)	−2.6369	0.045(3)	2350.03(1)	27.21	13.94
28	1965.49(1)	393.677(1)	−3.5175	0.069(3)	2355.72(1)	32.90	16.16
30	1929.40(1)	437.185(1)	−4.6007	0.101(2)	2362.09(1)	39.27	18.55
32	1892.81(1)	482.164(1)	−5.9161	0.138(2)	2369.20(1)	46.38	21.11
34	1855.79(1)	528.596(2)	−7.4957	0.188(2)	2377.08(1)	54.26	23.83
36	1818.41(1)	576.469(2)	−9.3738	0.249(2)	2385.75(1)	62.93	26.72
38	1780.74(1)	625.781(2)	−11.5878(1)	0.324(2)	2395.25(1)	72.43	29.77
40	1742.85(1)	676.538(2)	−14.1780(1)	0.410(2)	2405.62(1)	82.80	32.98
42	1704.80(1)	728.750(2)	−17.1871(1)	0.527(2)	2416.89(1)	94.08	36.37
44	1666.66(1)	782.439(2)	−20.6636(1)	0.658(3)	2429.09(1)	106.27	39.91
46	1628.474(6)	837.632(2)	−24.6586(1)	0.819(3)	2442.27(1)	119.45	43.62
48	1590.283(6)	894.359(2)	−29.2269(2)	1.006(4)	2456.42(1)	133.60	47.50
50	1552.163(6)	952.664(2)	−34.4303(2)	1.225(4)	2471.62(1)	148.80	51.54
52	1514.152(6)	1012.586(2)	−40.3321(3)	1.480(4)	2487.89(1)	165.07	55.74
54	1476.302(6)	1074.185(2)	−47.0071(2)	1.775(4)	2505.26(1)	182.44	60.11
56	1438.667(6)	1137.516(3)	−54.5316(4)	2.115(4)	2523.77(1)	200.95	64.65
58	1401.293(6)	1202.652(3)	−62.9927(6)	2.505(5)	2543.46(1)	220.64	69.35
60	1364.233(6)	1269.662(3)	−72.4831(7)	2.950(5)	2564.36(1)	241.54	74.22
62	1327.543(6)	1338.586(3)	−83.0822(7)	3.454(6)	2586.50(1)	263.68	79.25
64	1291.268(6)	1409.583(3)	−94.9364(7)	4.025(6)	2609.94(1)	287.12	84.44
66	1255.465(6)	1482.722(3)	−108.154(1)	4.656(6)	2634.69(2)	311.87	89.80
67	1237.756(6)	1520.147(3)	−115.331(1)	5.007(6)	2647.58(2)	324.76	92.54
68	1220.187(6)	1558.134(3)	−122.884(1)	5.392(6)	2660.83(2)	338.01	95.34
70	1185.496(6)	1635.896(4)	−139.249(1)	6.203(6)	2688.34(2)	365.53	101.02
72	1151.447(6)	1716.185(4)	−157.445(1)	7.108(6)	2717.29(2)	394.48	106.87
74	1118.102(6)	1799.133(5)	−177.646(1)	8.115(8)	2747.70(2)	424.88	112.89

TABLE IV. (*Continued*).

Z	$g_{j,\mathrm{SE}}$ ve + WF, red	$g_{j,\mathrm{SE}}$ WF, irred	$g_{j,\mathrm{VP}}$ WF	$g_{j,\mathrm{VP}}$ pot	Tot. $g_{j,\mathrm{QED}}$ (order α/π)	Effect of binding (total)	($Z\alpha$ exp)
75	1101.712(6)	1841.693(9)	−188.587(1)	8.665(8)	2763.48(2)	440.66	115.96
76	1085.527(6)	1884.879(9)	−200.047(1)	9.239(9)	2779.60(2)	456.78	119.08
77	1069.549(6)	1928.891(9)	−212.163(2)	9.845(9)	2796.12(3)	473.30	122.23
78	1053.790(6)	1973.625(9)	−224.886(2)	10.48(1)	2813.01(3)	490.19	125.43
79	1038.259(6)	2019.17(1)	−238.298(2)	11.15(1)	2830.29(3)	507.47	128.66
80	1022.963(6)	2065.50(1)	−252.387(2)	11.86(1)	2847.93(3)	525.11	131.94
81	1007.911(6)	2112.69(1)	−267.231(2)	12.60(1)	2865.96(3)	543.14	135.26
82	993.115(6)	2160.73(1)	−282.842(2)	13.37(1)	2884.38(3)	561.56	138.62
83	978.585(5)	2209.65(1)	−299.252(2)	14.19(1)	2903.18(3)	580.36	142.02
86	936.687(5)	2361.99(1)	−353.736(2)	16.88(1)	2961.83(3)	639.01	152.47
88	897.312(5)	2468.68(1)	−395.028(2)	18.90(1)	2989.87(3)	667.05	159.65
90	885.177(5)	2579.17(1)	−440.290(2)	21.11(1)	3045.16(3)	722.34	166.99
92	861.485(5)	2694.56(1)	−490.638(2)	23.52(1)	3088.93(3)	766.11	174.49
94	839.328(5)	2815.75(1)	−547.079(2)	26.18(1)	3134.18(3)	811.36	182.16

were taken from Refs. [103,117–119], and the radius of the most abundant or longest living isotope was employed, as indicated in Table V. The uncertainty caused by an insufficient knowledge of the nuclear radius is indicated in Fig. 10, where also all the other contributions to g_j are displayed. The recoil correction was calculated employing Eq. (99). Again, the mass of the most abundant isotope was utilized which causes the wiggles in the curve. Note that this correction can be considered as only an order of magnitude estimate for high Z. For carbon, we estimate its accuracy being 1%, decreasing with increasing Z and amounting to 10% already for calcium. Due to the rather speculative nature of both the uncertainty of this contribution and the estimate of the higher order QED contributions, an error for the total g_j value is not displayed in Table V. It amounts to at least 7×10^{-9} for carbon, 1.3×10^{-7} for calcium and 7×10^{-6} for uranium, where we have estimated the uncertainty from the uncalculated QED $(\alpha/\pi)^2$ binding corrections by 2.5 $\times(\alpha/\pi)$ times the numerical value of the (α/π) contribution. Contrary to the Lamb shift situation, however, this error margin is not due to nuclear effects which can hardly be estimated to increase in precision [1] but to yet uncalculated contributions, e.g., from the diagrams shown in Fig. 6. The error due to the uncertainty in $r_{\mathrm{rms}}=5.8604\pm0.0023$ fm [117] is also shown for uranium. It is smaller than the estimate for the yet uncalculated QED terms of order $(\alpha/\pi)^2$. The influence of nuclear mass and size effects is also demonstrated by the difference of the corresponding values for $^{207}\mathrm{Pb}^{81+}$ and $^{208}\mathrm{Pb}^{81+}$. Values are specified in Table V for both nuclei, and although their radii differ only by about 0.1%, this leads to a difference in g_j of 10^{-6}. The effect of the nuclear size on the QED correction itself was already mentioned. For the two different radii employed, the total QED value is the same within its error margins. When employing pointlike nuclei, however, the need for consideration

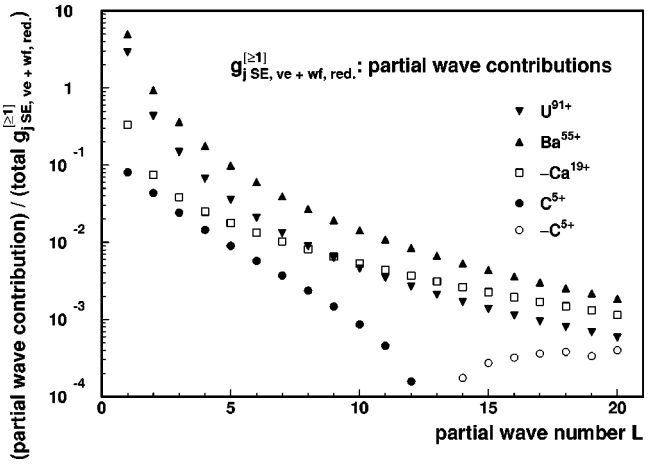

FIG. 7. Partial wave contributions $g^{[\geq1]}_{j,\mathrm{SE,ve}}+g^{[\geq1]}_{j,\mathrm{SE,WF,red}}$ for different Z.

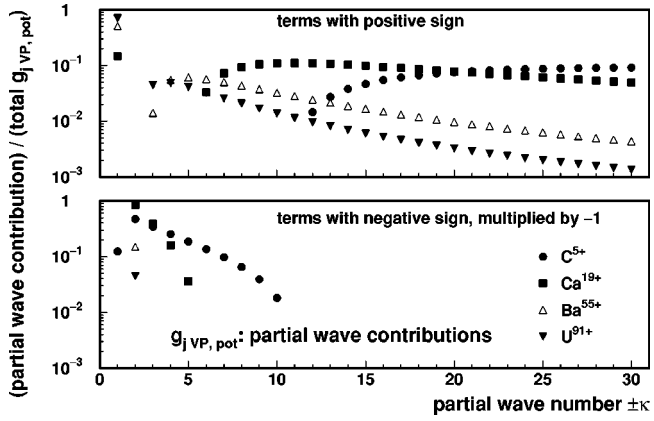

FIG. 8. Partial wave contributions to $g_{j\mathrm{VP,pot}}$. Each point represents the sum of contributions from κ and $-\kappa$. The top panel indicates the partial wave contributions with positive sign, the bottom panel those with negative sign. For C^{5+}, the total contribution $g_{j\mathrm{VP,pot}}$ was assumed to be 1×10^{-10} for calculation purposes.

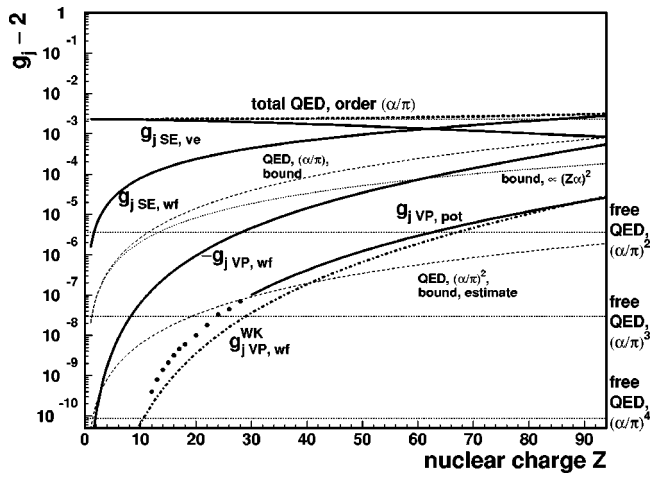

FIG. 9. The QED contributions to g_j, including the contributions from free QED up to order $(\alpha/\pi)^4$. The binding contribution of order (α/π) (see Table IV) is indicated separately, as well as the value of the $Z\alpha$ expansion due to Grotch [39] [''bound, $\propto(Z\alpha)^2$''] and the estimate for the bound-state effects of order $(\alpha/\pi)^2$. For $g_{j,\mathrm{VP,WF}}$, the negative value of this contribution is given.

of nuclear size effects in QED calculations for high Z is demonstrated impressively.

VI. COMPARISON WITH EXPERIMENTS

Up to now, experiments on g_j factors in hydrogenlike systems were carried out only for a few Z. We present an overview of these experiments in Table VI. The experiments carried out on H, D, and He^+ were all performed before 1980 and did not prove any effects beyond the $(\alpha/\pi)(Z\alpha)^2/6$ term or the ratio of the recoil predictions for H and D [44]. On the high-Z end of the periodic table, lifetime measurements of the hyperfine transitions in hydrogenlike ions were carried out only for $^{207}Pb^{81+}$ [17] and $^{209}Bi^{82+}$ [14,120], for which also theoretical calculations exist [19,20,53,121]. As Shabaev pointed out [53], the transition probability $1/\tau_{F\to F'}=\omega_{F\to F'}$ from the higher hyperfine niveau F to the lower, F' is in hydrogenlike ions related to g_j by

$$\omega_{F_2\to F_1}=\frac{\alpha}{3}\frac{(\Delta E_{\mathrm{HFS}})^3}{\hbar(m_e c^2)^2}\frac{I}{2I+1}\left[g_j^{(\mathrm{electron})}-\left(\frac{m_e}{m_p}\right)g_I^{(\mathrm{nucleus})}\right]^2, \tag{107}$$

where I is the nuclear spin and m_p is the proton mass. The constants $\hbar$, m_e, and c are explicitly displayed here.

The only recent experiment primarily designed for g_j measurements [47–49,122] was carried out on C^{5+} and yielded an impressive precision of about 10^{-9} which is certainly sufficient to distinguish between the full QED calculation of order α and Grotch's $(\alpha/\pi)(Z\alpha)^2/6$ term. Within the specified error margins, the experimental result and our calculation agree, and both uncertainties are of the same order of magnitude. An experiment with a similar precision for a heavier nucleus, however, could not match a similar theoretical prediction due to the yet uncalculated higher order effects of QED and recoil.

In order to elucidate the experimental capabilities, we display in Fig. 11 the magnitude of various contributions in parts of g_j as well as the experimental precision reached so far for the various Z. Thus, each theoretical curve crossed by the line of an experiment is checked by this experiment. It is worth mentioning that the experiment carried out on H by Tiedeman and Robinson [45] was almost as precise as that of Quint and co-workers on C^{5+}, but could just prove the binding effect of order $(Z\alpha)^2$ whereas the carbon experiment not only clearly pointed out the difference between this term and the full binding correction but also almost reached the current theoretical limits due to the already much stronger binding effects in carbon. These are indicated again by the curve denoted ''bound QED, $(\alpha/\pi)^2$, estimate.'' The area on the right under this curve has to be considered as theoretically unknown. For comparison, also the first and the best g factor measurement for a free electron are displayed in Fig. 11.

VII. CONCLUSION

We have presented the first complete calculation scheme for the g_j factor of an electron bound in a hydrogenlike system, including all QED corrections of order (α/π) nonperturbatively and thus valid for the whole Z range. All values are listed for a tight lattice of Z, in addition to all contributions of non-QED origin known so far. Error margins for both the calculated QED corrections as well as for the other contributions are properly estimated. Comparison with the existing experimental results exhibits agreement and sufficient precision in all cases. The finite nuclear size effect was found to be considerable for the QED corrections of order (α/π) in high-Z systems. The uncertainty of nuclear size and shape is well under control as it does not affect our predictions at the current level of precision. For further high precision experiments carried out in systems heavier than C^{5+}, it is desirable to evaluate all QED corrections of order $(\alpha/\pi)^2$ nonperturbatively as the next step.

ACKNOWLEDGMENTS

Valuable discussions with a large number of scholars are gratefully acknowledged, in particular with W. Quint, who provided experimental results with continuously increasing precision prior to publication, and also with E. E. B. Campbell, H.-J. Kluge, A.-M. Mårtensson-Pendrill, V. M. Shabaev, G. Soff, S. Stahl, J. Verdú, G. Werth, and V. A. Yerokhin, who showed permanent encouraging interest in our work. Financial support was obtained from the European Union (Contract No. ERB FMRX CT 97-0144) and the Swedish NFR.

APPENDIX A: FREE VERTEX FUNCTION $\Gamma^{[0]}(p,p')$

The free vertex function, Eq. (38), can be expressed in the Feynman gauge as

TABLE V. Known contributions to g_j for a $1s_{1/2}$ electron bound in a hydrogenlike ion. The employed nuclear rms radius is indicated. The last column displays the sum of all the others plus the free QED contributions of orders $(\alpha/\pi)^2$ to $(\alpha/\pi)^4$ and includes therefore all contributions known today. The value is not accurate to the digits specified, as yet unknown effects such as bound QED effects of order $(\alpha/\pi)^2$ or the complete recoil correction beyond the $Z\alpha$ expansion are not yet evaluated but might contribute on a level up to a few times 10^{-6}. A detailed discussion is given in the text. The numerical errors of the finite nuclear size contribution as well as the recoil contribution are always less than the last figure stated.

	$r_{\rm rms}$ [fm]	Rel. spin-orbit coupl.	Fin. nucl. size correction	Total QED, order α/π	Recoil correction	Total g_j
$^{1}_{1}$H	0.862	1.9999644986	$<1.\times10^{-11}$	$2.322840(1)\times10^{-3}$	2.9158×10^{-8}	2.002283853
$^{4}_{2}$He	1.671	1.9998579888	$<1.\times10^{-11}$	$2.322904(1)\times10^{-3}$	2.9178×10^{-8}	2.002177407
$^{7}_{3}$Li	2.410	1.9996804535	$4.\times10^{-11}$	$2.323013(1)\times10^{-3}$	3.7518×10^{-8}	2.001999989
$^{9}_{4}$Be	2.390	1.9994318644	$9.\times10^{-11}$	$2.323173(1)\times10^{-3}$	5.1878×10^{-8}	2.001751575
$^{11}_{5}$B	2.370	1.9991121817	1.9×10^{-10}	$2.323389(1)\times10^{-3}$	6.6321×10^{-8}	2.001432122
$^{12}_{6}$C	2.468	1.9987213542	4.2×10^{-10}	$2.323664(1)\times10^{-3}$	8.7542×10^{-8}	2.001041591
$^{14}_{7}$N	2.560	1.9982593193	8.3×10^{-10}	$2.324004(1)\times10^{-3}$	1.0213×10^{-7}	2.000579911
$^{16}_{8}$O	2.693	1.9977260027	1.56×10^{-9}	$2.324416(1)\times10^{-3}$	1.1672×10^{-7}	2.000047022
$^{19}_{9}$F	2.898	1.9971213189	2.90×10^{-9}	$2.324903(1)\times10^{-3}$	1.2441×10^{-7}	1.999442834
$^{20}_{10}$Ne	3.006	1.9964451704	4.78×10^{-9}	$2.325472(1)\times10^{-3}$	1.4591×10^{-7}	1.998767278
$^{23}_{11}$Na	2.994	1.9956974482	6.99×10^{-9}	$2.326130(1)\times10^{-3}$	1.5352×10^{-7}	1.998020224
$^{24}_{12}$Mg	3.057	1.9948780313	1.040×10^{-8}	$2.326881(2)\times10^{-3}$	1.7509×10^{-7}	1.997201582
$^{27}_{13}$Al	3.063	1.9939867870	1.451×10^{-8}	$2.327729(2)\times10^{-3}$	1.8266×10^{-7}	1.996311199
$^{28}_{14}$Si	3.123	1.9930235706	2.047×10^{-8}	$2.328682(2)\times10^{-3}$	2.0427×10^{-7}	1.995348962
$^{31}_{15}$P	3.190	1.9919882250	2.842×10^{-8}	$2.329742(3)\times10^{-3}$	2.1180×10^{-7}	1.994314692
$^{32}_{16}$S	3.263	1.9908805811	3.890×10^{-8}	$2.330920(3)\times10^{-3}$	2.3345×10^{-7}	1.993208259
$^{35}_{17}$Cl	3.388	1.9897004574	5.402×10^{-8}	$2.332216(3)\times10^{-3}$	2.4096×10^{-7}	1.992029453
$^{40}_{18}$Ar	3.427	1.9884476596	7.028×10^{-8}	$2.333636(4)\times10^{-3}$	2.3638×10^{-7}	1.990778087
$^{40}_{20}$Ca	3.478	1.9857232017	1.1315×10^{-7}	$2.33692(1)\times10^{-3}$	2.9182×10^{-7}	1.98805701
$^{48}_{22}$Ti	3.592	1.9827053968	1.8151×10^{-7}	$2.34062(1)\times10^{-3}$	2.9426×10^{-7}	1.98504298
$^{52}_{24}$Cr	3.645	1.9793922218	2.7264×10^{-7}	$2.34502(1)\times10^{-3}$	3.2325×10^{-7}	1.98173433
$^{56}_{26}$Fe	3.738	1.9757814341	4.0742×10^{-7}	$2.35003(1)\times10^{-3}$	3.5227×10^{-7}	1.97812871
$^{58}_{28}$Ni	3.776	1.9718705637	5.7841×10^{-7}	$2.35572(1)\times10^{-3}$	3.9446×10^{-7}	1.97422374
$^{64}_{30}$Zn	3.928	1.9676569044	8.5363×10^{-7}	$2.36209(1)\times10^{-3}$	4.1038×10^{-7}	1.97001674
$^{74}_{32}$Ge	4.072	1.9631375039	1.23126×10^{-6}	$2.36920(1)\times10^{-3}$	4.0383×10^{-7}	1.96550482
$^{80}_{34}$Se	4.140	1.9583091529	1.68661×10^{-6}	$2.37708(1)\times10^{-3}$	4.2169×10^{-7}	1.96068482
$^{84}_{36}$Kr	4.188	1.9531683728	2.26079×10^{-6}	$2.38575(1)\times10^{-3}$	4.5025×10^{-7}	1.95555332
$^{88}_{38}$Sr	4.224	1.9477114023	2.98196×10^{-6}	$2.39525(1)\times10^{-3}$	4.7886×10^{-7}	1.95010660
$^{90}_{40}$Zr	4.270	1.9419341826	3.91435×10^{-6}	$2.40562(1)\times10^{-3}$	5.1880×10^{-7}	1.94434072
$^{98}_{42}$Mo	4.407	1.9358323401	5.30150×10^{-6}	$2.41689(1)\times10^{-3}$	5.2529×10^{-7}	1.93825155
$^{102}_{44}$Ru	4.481	1.9294011690	6.92783×10^{-6}	$2.42909(1)\times10^{-3}$	5.5390×10^{-7}	1.93183423
$^{106}_{46}$Pd	4.532	1.9226356104	8.90456×10^{-6}	$2.44227(1)\times10^{-3}$	5.8256×10^{-7}	1.92508385
$^{114}_{48}$Cd	4.610	1.9155302297	1.150273×10^{-5}	$2.45642(1)\times10^{-3}$	5.8981×10^{-7}	1.91799523
$^{120}_{50}$Sn	4.655	1.9080791919	1.458117×10^{-5}	$2.47162(1)\times10^{-3}$	6.0798×10^{-7}	1.91056249
$^{130}_{52}$Te	4.742	1.9002762337	1.870057×10^{-5}	$2.48789(1)\times10^{-3}$	6.0702×10^{-7}	1.90277991
$^{132}_{54}$Xe	4.787	1.8921146327	2.348835×10^{-5}	$2.50526(1)\times10^{-3}$	6.4469×10^{-7}	1.89464051
$^{138}_{56}$Ba	4.839	1.8835871727	2.946784×10^{-5}	$2.52377(1)\times10^{-3}$	6.6318×10^{-7}	1.88613756
$^{140}_{58}$Ce	4.877	1.8746861060	3.665128×10^{-5}	$2.54346(1)\times10^{-3}$	7.0123×10^{-7}	1.87726340
$^{142}_{60}$Nd	4.914	1.8654031102	4.543511×10^{-5}	$2.56436(1)\times10^{-3}$	7.3985×10^{-7}	1.86801013
$^{152}_{62}$Sm	5.092	1.8557292402	5.904250×10^{-5}	$2.58650(1)\times10^{-3}$	7.3803×10^{-7}	1.85837201
$^{158}_{64}$Gd	5.159	1.8456548742	7.352327×10^{-5}	$2.60994(1)\times10^{-3}$	7.5655×10^{-7}	1.84833558
$^{164}_{66}$Dy	5.224	1.8351696537	9.127150×10^{-5}	$2.63469(2)\times10^{-3}$	7.7514×10^{-7}	1.83789287
$^{165}_{67}$Ho	5.210	1.8297695177	1.0005880×10^{-4}	$2.64758(2)\times10^{-3}$	7.9397×10^{-7}	1.83251443
$^{166}_{68}$Er	5.250	1.8242624144	1.1162833×10^{-4}	$2.66083(2)\times10^{-3}$	8.1291×10^{-7}	1.82703217
$^{174}_{70}$Yb	5.317	1.8129211091	1.3813825×10^{-4}	$2.68834(2)\times10^{-3}$	8.2183×10^{-7}	1.81574490
$^{178}_{72}$Hf	5.349	1.8011327199	1.6878208×10^{-4}	$2.71729(2)\times10^{-3}$	8.4993×10^{-7}	1.80401613
$^{184}_{74}$W	5.373	1.7888831574	2.0549106×10^{-4}	$2.74770(2)\times10^{-3}$	8.6853×10^{-7}	1.79183371

TABLE V. (*Continued*).

	$r_{\rm rms}$ [fm]	Rel. spin-orbit coupl.	Fin. nucl. size correction	Total QED, order α/π	Recoil correction	Total g_j
$^{187}_{75}$Re	5.351	1.7825807127	2.2430321×10^{-4}	$2.76348(2)\times10^{-3}$	8.7785×10^{-7}	1.78556586
$^{192}_{76}$Os	5.406	1.7761571469	2.5067037×10^{-4}	$2.77960(2)\times10^{-3}$	8.7794×10^{-7}	1.77918478
$^{193}_{77}$Ir	5.401	1.7696103440	2.7498925×10^{-4}	$2.79612(3)\times10^{-3}$	8.9652×10^{-7}	1.77267884
$^{195}_{78}$Pt	5.427	1.7629380960	3.0447120×10^{-4}	$2.81301(3)\times10^{-3}$	9.1053×10^{-7}	1.76605297
$^{197}_{79}$Au	5.437	1.7561380981	3.3542557×10^{-4}	$2.83029(3)\times10^{-3}$	9.2454×10^{-7}	1.75930122
$^{202}_{80}$Hg	5.467	1.7492079430	3.7174013×10^{-4}	$2.84793(3)\times10^{-3}$	9.2463×10^{-7}	1.75242502
$^{205}_{81}$Tl	5.483	1.7421451145	4.1020883×10^{-4}	$2.86596(3)\times10^{-3}$	9.3402×10^{-7}	1.74541871
$^{208}_{82}$Pb	5.504	1.7349469812	4.5324540×10^{-4}	$2.88438(3)\times10^{-3}$	9.4342×10^{-7}	1.73828204
$^{207}_{82}$Pb	5.497	1.7349469812	4.5234899×10^{-4}	$2.88438(3)\times10^{-3}$	9.4797×10^{-7}	1.73828114
$^{209}_{83}$Bi	5.533	1.7276107891	5.0197187×10^{-4}	$2.90318(3)\times10^{-3}$	9.6194×10^{-7}	1.73101338
$^{222}_{86}$Rn	5.632	1.7047443147	6.8357303×10^{-4}	$2.96183(3)\times10^{-3}$	9.7226×10^{-7}	1.70838717
$^{226}_{88}$Ra	5.662	1.6887529452	8.3147083×10^{-4}	$2.98987(3)\times10^{-3}$	9.9999×10^{-7}	1.69257177
$^{232}_{90}$Th	5.802	1.6721308209	1.0408652×10^{-3}	$3.04516(3)\times10^{-3}$	1.0189×10^{-6}	1.67621435
$^{238}_{92}$U	5.860	1.6548461126	1.2752380×10^{-3}	$3.08893(3)\times10^{-3}$	1.0379×10^{-6}	1.65920780
$^{244}_{94}$Pu	5.794	1.6368634079	1.5157404×10^{-3}	$3.13418(3)\times10^{-3}$	1.0568×10^{-6}	1.64151087

$$\Gamma_\mu^{[0]}(\mathrm{p},\mathrm{p}') = \frac{e^2}{(4\pi)^2}\{\gamma_\mu[4C_{24}-2+2m_e^2C_0-4\mathrm{pp}'(C_0+C_{11}+C_{12}+C_{23})-2\mathrm{p}^2(C_{11}+C_{21})-2\mathrm{p}'^2(C_{12}+C_{22})]$$
$$+\not{p}\mathrm{p}_\mu[4(C_{11}+C_{21})]+\not{p}\mathrm{p}'_\mu[4(C_0+C_{11}+C_{12}+C_{23})]+\not{p}'\mathrm{p}_\mu[4(C_0+C_{11}+C_{12}+C_{23})]$$
$$+\not{p}'\mathrm{p}'_\mu[4(C_{12}+C_{22})]-\not{p}\gamma_\mu\not{p}'[2(C_0+C_{11}+C_{12})]-\mathrm{p}_\mu[4m_e(C_0+2C_{11})]-\mathrm{p}'_\mu[4m_e(C_0+2C_{12})]\}, \tag{A1}$$

where the coefficient functions C_{ij} denote Feynman parameter integrals. These integrals can be written as (note some misprint corrections compared to Ref. [74] and a slightly different notation in Ref. [93])

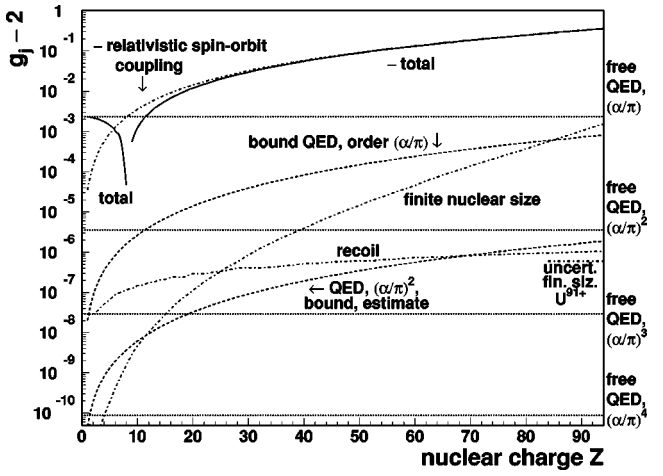

FIG. 10. All known contributions to g_j of the $1s_{1/2}$ state of a hydrogenlike ion, including recoil and finite nuclear size. For $Z \geqslant 9$, the total value of g_j is <2, and therefore ''-total'' is displayed for these Z. The uncertainty due to the error margins of the uranium rms radius are also indicated.

$$m_e^2C_0 = \int_0^1 dy\,\frac{1}{a}\ln\left(\frac{a+b}{b}\right), \tag{A2}$$

$$m_e^2C_{11} = -\int_0^1 dy\,\frac{y}{a}\left[1-\frac{b}{a}\ln\left(\frac{a+b}{b}\right)\right], \tag{A3}$$

$$m_e^2C_{12} = -\int_0^1 dy\,\frac{1-y}{a}\left[1-\frac{b}{a}\ln\left(\frac{a+b}{b}\right)\right], \tag{A4}$$

$$m_e^2C_{21} = \int_0^1 dy\,\frac{y^2}{a}\left[\frac{1}{2}-\frac{b}{a}+\left(\frac{b}{a}\right)^2\ln\left(\frac{a+b}{b}\right)\right], \tag{A5}$$

$$m_e^2C_{22} = \int_0^1 dy\,\frac{(1-y)^2}{a}\left[\frac{1}{2}-\frac{b}{a}+\left(\frac{b}{a}\right)^2\ln\left(\frac{a+b}{b}\right)\right], \tag{A6}$$

$$m_e^2C_{23} = \int_0^1 dy\,\frac{y(1-y)}{a}\left[\frac{1}{2}-\frac{b}{a}+\left(\frac{b}{a}\right)^2\ln\left(\frac{a+b}{b}\right)\right], \tag{A7}$$

TABLE VI. Experimental results for g_j in hydrogenlike systems. For hydrogen and deuterium, only more recent results are listed, references to older experiments can be found in Refs. [43–45]. Experimental techniques are abbreviated as SEOP (spin-exchange optical pumping), HFHM (high-field double mode hydrogen maser), PT (penning trap), and HFST (hyperfine splitting transition). The ratio of $g_j(\mathrm{H})/g_j(\mathrm{D})$ is more precisely known as each of the g_j factors due to the uncertainty in the QED calculations.

		Measured quantity	g_j(expt.)	g_j(theory)	Method	Ref.
^{1}H	$g_j(\mathrm{H})/g_j(\mathrm{e}^-)$	$=1-17.4(1.0)\times10^{-6}$	2.002 284(2)	2.002 283 853	SEOP	[43]
^{1}H	$g_j(\mathrm{H})/g_j(\mathrm{e}^-)$	$=1-17.709(13)\times10^{-6}$	2.002 283 845(26)	2.002 283 853	SEOP	[45]
^{2}D	$g_j(\mathrm{H})/g_j(\mathrm{D})$	$=1+7.22(3)\times10^{-9}$		$(1+7.221\times10^{-9})$[a]	HFHM	[44]
^{4}He$^+$	$g_j(\mathrm{He}^+)/g_j(\mathrm{e}^-)$	$=1-70.87(30)\times10^{-6}$	2.002 177 4(60)	2.002 177 407	SEOP	[46]
^{12}C^{5+}	$g_j(\mathrm{C}^{5+})$		2.001 042(2)	2.001 041 591(7)[b]	PT	[49]
^{12}C^{5+}	$g_j(\mathrm{C}^{5+})$		2.001 041 596(5)	2.001 041 591(7)[b]	PT	[122]
^{207}Pb^{81+}	$\tau_{F\to F'}(\mathrm{Pb}^{81+})$	$=49.5(6.5)$ ms	1.78(12)	1.738 281 14	HFST	[17,53]
^{209}Bi^{82+}	$\tau_{F\to F'}(\mathrm{Bi}^{82+})$	$=0.3975(15)$ ms	1.7341(35)	1.731 013 38	HFST	[120]

[a]Value obtained from the ratio of the recoil contributions.
[b]Estimate for the total theoretical uncertainty; see text.

$$C_{24}=\frac{1}{4}\left\{\Delta+1-\int_0^1 dy\,\frac{b}{a}\left[1-\frac{b}{a}\ln\left(\frac{a+b}{b}\right)\right]-\int_0^1 dy\,\ln(a+b)\right\} \tag{A8}$$

In C_{24}, Δ denotes again the ultraviolet part of the charge renormalization constant (35). The auxiliary functions read

$$b=y\rho-(1-y)\rho', \tag{A9}$$

$$a+b=1-y(1-y)q^2/m_e^2, \tag{A10}$$

$$q=p-p', \tag{A11}$$

$$\Delta=2/\epsilon-\gamma_E+\ln 4\pi. \tag{A12}$$

The prime $'$ denotes quantities related to p' in Eq. (38).

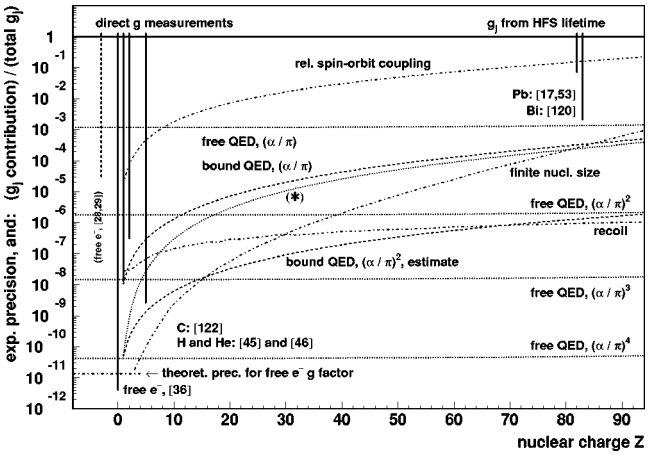

FIG. 11. Precision of *g*-factor experiments compared to the relative value of different contributions to g_j. The curve marked with an asterisk indicates the difference between the $(\alpha/\pi)(Z\alpha)^2/6$ term by Grotch [39] and the full bound state QED calculation of order (α/π).

APPENDIX B: ANGULAR FACTORS $\mathcal{A}$

The angular factors of Eqs. (67) and (77) read

$$\mathcal{A}^0_{\mathrm{SE}}(n,p;l)=(2j_p+1)\begin{pmatrix} j_p & j_n & l \\ \frac{1}{2} & -\frac{1}{2} & 0\end{pmatrix}^2, \tag{B1}$$

$$\mathcal{A}^i_{\mathrm{SE}}(n,p;l)=(-1)^{l_s+l_p+1}6(2j_p+1)\sum_k (2k+1)\times\begin{pmatrix} k & j_n & l \\ \frac{1}{2} & -\frac{1}{2} & 0\end{pmatrix}\begin{pmatrix} j_p & k & l \\ \frac{1}{2} & -\frac{1}{2} & 0\end{pmatrix}\times\begin{Bmatrix} j_p & 1 & k \\ \frac{1}{2} & l_\alpha(i) & \frac{1}{2}\end{Bmatrix}\begin{Bmatrix} 1 & j_p & k \\ l_\beta(i) & \frac{1}{2} & \frac{1}{2}\end{Bmatrix}, \tag{B2}$$

where $l_\alpha(i)$ is the angular momentum related to $-\kappa_p$ for $i=1,2$ and related to κ_p for $i=3,4$. Similarly, l_β is related to κ_p for $i=2,3$ and to $-\kappa_p$ for $i=1,4$. The parentheses and curly braces denote $3j$ and $6j$ symbols, respectively.

For Eq. (80), the angular factors read

$$\mathcal{A}^0_{\mathrm{VE}}(n,q,r;l)=(-1)^{1+j_n+l_n+l_q+j_r}\times\sqrt{\frac{2j_n+1}{2j_n(j_n+1)}}(2j_q+1)(2j_r+1)\times\begin{pmatrix} j_r & j_q & 1 \\ -\frac{1}{2} & -\frac{1}{2} & 1\end{pmatrix}\begin{pmatrix} j_r & j_n & l \\ \frac{1}{2} & -\frac{1}{2} & 0\end{pmatrix}\times\begin{pmatrix} j_n & j_q & l \\ \frac{1}{2} & -\frac{1}{2} & 0\end{pmatrix}\begin{Bmatrix} j_n & j_r & l \\ j_q & j_n & 1\end{Bmatrix}, \tag{B3}$$

$$\mathcal{A}^{i}_{\mathrm{VE}}(n,q,r;l)=(-1)^{j_n+l_n+l_q+j_q}\sqrt{\frac{2j_n+1}{2j_n(j_n+1)}}(2j_q+1)(2j_r+1)\begin{pmatrix} j_q & j_r & 1\\ -\frac{1}{2} & -\frac{1}{2} & 1\end{pmatrix}6\sum_{k,k'}(2k+1)(2k'+1)\begin{pmatrix} k & j_n & l\\ \frac{1}{2} & -\frac{1}{2} & 0\end{pmatrix}$$
$$\times\begin{pmatrix} j_n & k' & l\\ \frac{1}{2} & -\frac{1}{2} & 0\end{pmatrix}\begin{Bmatrix} j_r & 1 & k\\ \frac{1}{2} & l_\alpha(i) & \frac{1}{2}\end{Bmatrix}\begin{Bmatrix} 1 & j_q & k'\\ l_\beta(i) & \frac{1}{2} & \frac{1}{2}\end{Bmatrix}\begin{Bmatrix} j_n & j_n & 1\\ k & k' & l\end{Bmatrix}\begin{Bmatrix} j_q & j_r & 1\\ k & k' & 1\end{Bmatrix}. \tag{B4}$$

As in Eq. (B2), $l_\alpha(i)$ is the angular momentum related to $-\kappa_q$ for $i=1,2$ and related to κ_q for $i=3,4$ and l_β to κ_q for $i=2,3$ and to $-\kappa_q$ for $i=1,4$.

The angular factors for Eq. (94) read

$$\mathcal{A}^{i}_{\mathrm{VP}}(\kappa_{a_n},\kappa,\kappa';l=1)=(-1)^{1+j_\kappa+j_{\kappa'}+l_\kappa+l_{\kappa'}}\sqrt{\frac{2j_{\kappa_{a_n}}}{2j_{\kappa_{a_n}}(j_{\kappa_{a_n}}+1)}}(2j_\kappa+1)(2j_{\kappa'}+1)$$
$$\times\begin{pmatrix} j_\kappa & j_{\kappa'} & 1\\ -\frac{1}{2} & -\frac{1}{2} & 1\end{pmatrix}6\sum_{k,k'}(2k+1)(2k'+1)\begin{pmatrix} k & j_{\kappa_{a_n}} & 1\\ \frac{1}{2} & -\frac{1}{2} & 0\end{pmatrix}\begin{pmatrix} j_{\kappa_{a_n}} & k' & 1\\ \frac{1}{2} & -\frac{1}{2} & 0\end{pmatrix}$$
$$\times\begin{Bmatrix} j_{\kappa_{a_n}} & 1 & k\\ \frac{1}{2} & l_\alpha(i) & \frac{1}{2}\end{Bmatrix}\begin{Bmatrix} 1 & j_\kappa & k'\\ l_\beta(i) & \frac{1}{2} & \frac{1}{2}\end{Bmatrix}\begin{Bmatrix} j_{\kappa_{a_n}} & j_{\kappa_{a_n}} & 1\\ 1 & 1 & k\end{Bmatrix}\begin{Bmatrix} j_{\kappa'} & j_\kappa & 1\\ 1 & 1 & k'\end{Bmatrix}. \tag{B5}$$

$l_\alpha(i)$ is the angular momentum related to $-\kappa_{a_n}$ for $i=1,2$ and related to κ_{a_n} for $i=3,4$ and l_β is related to κ for $i=2,4$ and to $-\kappa$ for $i=1,3$. The detailed evaluation of all these factors is presented in Ref. [95].

APPENDIX C: RADIAL INTEGRALS $\mathcal{Q},\mathcal{R},\mathcal{S},\mathcal{T},\mathcal{V},\mathcal{W}$

The radial integrals $\mathcal{Q},\mathcal{R},\mathcal{S},\mathcal{T},\mathcal{V},\mathcal{W}$ from Eqs. (67), (77), (80), and (94) read

$$\mathcal{Q}[(a,\kappa),(b,\kappa');k,l]=\int_{r=0}^{\infty}dr\,r^2 f_{a,\kappa}(r)j_l(kr)g_{b,\kappa'}(r), \tag{C1}$$

$$\mathcal{R}(a,b)=\int_{r=0}^{\infty}dr\,r^3[f_a(r)g_b(r)+g_a(r)f_b(r)], \tag{C2}$$

$$\mathcal{S}(a,b,c,d;k,l)=\left(\int_{r_1=0}^{\infty}dr_1 r_1^2[f_a(r_1)j_l(kr_1)f_b(r_1)+g_a(r_1)j_l(kr_1)g_b(r_1)]\right)\left(\int_{r_2=0}^{\infty}dr_2 r_2^2[f_c(r_2)j_l(kr_2)f_d(r_2)\right.$$
$$\left.+g_c(r_2)j_l(kr_2)g_d(r_2)]\right), \tag{C3}$$

$$\mathcal{T}(a,b,c,d;k,l)=\left(\int_{r_1=0}^{\infty}dr_1 r_1^2[f_a(r_1)j_l(kr_1)f_b(r_1)+g_a(r_1)j_l(kr_1)g_b(r_1)]\right)\left(\int_{r_3=0}^{\infty}dr_3 r_3^2 V^{\mathrm{bind}}_{\mathrm{nuc}}(r_3)[f_b(r_3)f_c(r_3)\right.$$
$$\left.+g_b(r_3)g_c(r_3)]\right)\left(\int_{r_2=0}^{\infty}dr_2 r_2^2[f_c(r_2)j_l(kr_2)f_d(r_2)+g_c(r_2)j_l(kr_2)g_d(r_2)]\right), \tag{C4}$$

$$\mathcal{V}^1(a,b,c,d;k,l)=\left(\int_{r_1=0}^{\infty}dr_1 r_1^2 f_a(r_1)j_l(kr_1)g_b(r_1)\right)\left(\int_{r_2=0}^{\infty}dr_2 r_2^2 g_c(r_2)j_l(kr_2)f_d(r_2)\right), \tag{C5}$$

$$\mathcal{V}^2(a,b,c,d;k,l)=\left(\int_{r_1=0}^{\infty}dr_1 r_1^2 f_a(r_1)j_l(kr_1)g_b(r_1)\right)\left(\int_{r_2=0}^{\infty}dr_2 r_2^2 f_c(r_2)j_l(kr_2)g_d(r_2)\right), \tag{C6}$$

$$\mathcal{V}^3(a,b,c,d;k,l)=\left(\int_{r_1=0}^{\infty}dr_1 r_1^2 g_a(r_1)j_l(kr_1)f_b(r_1)\right)\left(\int_{r_2=0}^{\infty}dr_2 r_2^2 f_c(r_2)j_l(kr_2)g_d(r_2)\right), \tag{C7}$$

$$\mathcal{V}^4(a,b,c,d;k,l)=\left(\int_{r_1=0}^{\infty} dr_1 r_1^2 g_a(r_1) j_l(kr_1) f_b(r_1)\right)\left(\int_{r_2=0}^{\infty} dr_2 r_2^2 g_c(r_2) j_l(kr_2) f_d(r_2)\right), \tag{C8}$$

$$\mathcal{W}^1(a,b,c,d;k,l)=\left(\int_{r_1=0}^{\infty} dr_1 r_1^2 f_a(r_1) j_l(kr_1) g_b(r_1)\right)\left(\int_{r_3=0}^{\infty} dr_3 r_3^2 V_{\rm nuc}^{\rm bind}(r_3)[f_b(r_3) f_b(r_3)+g_c(r_3) g_c(r_3)]\right)$$
$$\times\left(\int_{r_2=0}^{\infty} dr_2 r_2^2 g_c(r_2) j_l(kr_2) f_d(r_2)\right), \tag{C9}$$

$$\mathcal{W}^2(a,b,c,d;k,l)=\left(\int_{r_1=0}^{\infty} dr_1 r_1^2 f_a(r_1) j_l(kr_1) g_b(r_1)\right)\left(\int_{r_3=0}^{\infty} dr_3 r_3^2 V_{\rm nuc}^{\rm bind}(r_3)[f_b(r_3) f_c(r_3)+g_b(r_3) g_c(r_3)]\right)$$
$$\times\left(\int_{r_2=0}^{\infty} dr_2 r_2^2 f_c(r_2) j_l(kr_2) g_d(r_2)\right), \tag{C10}$$

$$\mathcal{W}^3(a,b,c,d;k,l)=\left(\int_{r_1=0}^{\infty} dr_1 r_1^2 g_a(r_1) j_l(kr_1) f_b(r_1)\right)\left(\int_{r_3=0}^{\infty} dr_3 r_3^2 V_{\rm nuc}^{\rm bind}(r_3)[f_b(r_3) f_c(r_3)+g_b(r_3) g_c(r_3)]\right)$$
$$\times\left(\int_{r_2=0}^{\infty} dr_2 r_2^2 f_c(r_2) j_l(kr_2) g_d(r_2)\right), \tag{C11}$$

$$\mathcal{W}^4(a,b,c,d;k,l)=\left(\int_{r_1=0}^{\infty} dr_1 r_1^2 g_a(r_1) j_l(kr_1) f_b(r_1)\right)\left(\int_{r_3=0}^{\infty} dr_3 r_3^2 V_{\rm nuc}^{\rm bind}(r_3)[f_b(r_3) f_c(r_3)+g_b(r_3) g_c(r_3)]\right)$$
$$\times\left(\int_{r_2=0}^{\infty} dr_2 r_2^2 g_c(r_2) j_l(kr_2) f_d(r_2)\right) \tag{C12}$$

In these equations, f and g denote large and small radial component of the wave functions

$$\Phi_a(\mathbf{r})=\begin{pmatrix} f_{a,\kappa}(r)\chi_{\kappa_a}^m(\hat{\mathbf{r}}) \\ ig_{a,\kappa}(r)\chi_{-\kappa_a}^m(\hat{\mathbf{r}}) \end{pmatrix} \tag{C13}$$

with $r=|\mathbf{r}|$. The indices a,b,c,d in Eqs. (C3)–(C12) have to be considered here as cumulative quantum numbers, i.e., the angular momentum quantum number is not specified separately (except for $\mathcal{Q}$).

APPENDIX D: THE FUNCTION $G(s,t,u)$

The denominator of Eq. (81) is contained in

$$\begin{aligned}
G(s,t,u)&=[2k(E_n-E_s-k)(E_n-E_t-k)(E_n-E_u-k)]^{-1} \quad E_s>0,\ E_t>0,\ E_u>0,\\
&=[2k(E_n-E_s-k)(E_n-E_t-k)(E_n-E_u+k)]^{-1}+[(E_t-E_u)(E_n-E_s-k)(E_n-E_t-k)(E_n-E_u+k)]^{-1}\\
&\quad -[(E_t-E_u)(E_p-E_u)(E_n-E_s-k)(E_n-E_u+k)]^{-1} \quad E_s>0,\ E_t>0,\ E_u<0,\\
&=[2k(E_n-E_s-k)(E_n-E_t+k)(E_n-E_u-k)]^{-1}+[(E_u-E_t)(E_n-E_s-k)(E_n-E_t+k)(E_n-E_u-k)]^{-1}\\
&\quad -[(E_u-E_t)(E_s-E_t)(E_n-E_s-k)(E_n-E_t+k)]^{-1} \quad E_s>0,\ E_t<0,\ E_u>0,\\
&=[2k(E_n-E_s+k)(E_n-E_t-k)(E_n-E_u-k)]^{-1}+[(E_t-E_s)(E_n-E_u-k)(E_n-E_t-k)(E_n-E_s+k)]^{-1}\\
&\quad -[(E_t-E_s)(E_u-E_s)(E_n-E_u-k)(E_n-E_s+k)]^{-1} \quad E_s<0,\ E_t>0,\ E_u>0,\\
&=[2k(E_n-E_s+k)(E_n-E_t+k)(E_n-E_u-k)]^{-1}+[(E_u-E_t)(E_n-E_s+k)(E_n-E_t+k)(E_n-E_u-k)]^{-1}\\
&\quad +[(E_u-E_t)(E_u-E_s)(E_n-E_s+k)(E_n-E_u-k)]^{-1} \quad E_s<0,\ E_t<0,\ E_u>0,\\
&=[2k(E_n-E_s+k)(E_n-E_t-k)(E_n-E_u+k)]^{-1}+[(E_t-E_u)(E_n-E_s+k)(E_n-E_t-k)(E_n-E_u+k)]^{-1}
\end{aligned}$$

$$
\begin{aligned}
&+[(E_t-E_u)(E_t-E_s)(E_n-E_s+k)(E_n-E_t-k)]^{-1} \quad E_s<0,\ E_t>0,\ E_u<0,\\
&=[2k(E_n-E_s-k)(E_n-E_t+k)(E_n-E_u+k)]^{-1}+[(E_s-E_t)(E_n-E_s-k)(E_n-E_t+k)(E_n-E_u+k)]^{-1}\\
&\quad +[(E_s-E_t)(E_s-E_u)(E_n-E_u+k)(E_n-E_s-k)]^{-1} \quad E_s>0,\ E_t<0,\ E_u<0,\\
&=[2k(E_n-E_s+k)(E_n-E_t+k)(E_n-E_u+k)]^{-1} \quad E_s<0,\ E_t<0,\ E_u<0. \qquad \text{(D1)}
\end{aligned}
$$

[1] P. J. Mohr, G. Plunien, and G. Soff, Phys. Rep. **293**, 227 (1998).

[2] H. F. Beyer and T. Stöhlker, in *Frontier Tests of QED and Physics of the Vacuum*, edited by E. Zavattini, D. Bakalov, and C. Rizzo (Heron, Sofia, 1998), pp. 356–370.

[3] J. Schweppe, A. Belkacem, L. Blumenfeld, N. Claytor, B. Feinberg, H. Gould, V. E. Kostroun, L. Levy, S. Misawa, J. R. Mowat, and M. H. Prior, Phys. Rev. Lett. **66**, 1434 (1991).

[4] P. Beiersdorfer, D. Knapp, R. E. Marrs, S. R. Elliott, and M. H. Chen, Phys. Rev. Lett. **71**, 3939 (1993).

[5] P. Beiersdorfer, A. Osterheld, S. R. Elliott, M. H. Chen, D. Knapp, and K. Reed, Phys. Rev. A **52**, 2693 (1995).

[6] P. Beiersdorfer, A. L. Osterheld, J. H. Scofield, J. R. Crespo López-Urrutia, and K. Widmann, Phys. Rev. Lett. **80**, 3022 (1998).

[7] U. Staude, P. Bosselmann, R. Büttner, D. Horn, K.-H. Schartner, F. Folkmann, A. E. Livingston, T. Ludziejewski, and P. H. Mokler, Phys. Rev. A **58**, 3516 (1998).

[8] P. Bosselmann, U. Staude, D. Horn, K.-H. Schartner, F. Folkmann, A. E. Livingston, and P. H. Mokler, Phys. Rev. A **59**, 1874 (1999).

[9] P. Indelicato and J. P. Desclaux, Phys. Rev. A **42**, 5139 (1990).

[10] Y. Kim, D. H. Baik, P. Indelicato, and J. P. Desclaux, Phys. Rev. A **44**, 148 (1991).

[11] S. A. Blundell, Phys. Rev. A **47**, 1790 (1993).

[12] A. Ynnerman, J. James, I. Lindgren, H. Persson, and S. Salomonson, Phys. Rev. A **50**, 4671 (1994).

[13] V. A. Yerokhin, A. N. Artemyev, T. Beier, G. Plunien, V. M. Shabaev, and G. Soff, Phys. Rev. A **60**, 3522 (1999).

[14] I. Klaft, S. Borneis, T. Engel, B. Fricke, R. Grieser, G. Huber, T. Kühl, D. Marx, R. Neumann, S. Schröder, P. Seelig, and L. Völker, Phys. Rev. Lett. **73**, 2425 (1994).

[15] J. R. Crespo López-Urrutia, P. Beiersdorfer, D. W. Savin, and K. Widmann, Phys. Rev. Lett. **77**, 826 (1996).

[16] J. R. Crespo López-Urrutia, P. Beiersdorfer, K. Widmann, B. B. Birkett, A.-M. Mårtensson-Pendrill, and M. G. H. Gustavsson, Phys. Rev. A **57**, 879 (1998).

[17] P. Seelig *et al.*, Phys. Rev. Lett. **81**, 4824 (1998).

[18] V. M. Shabaev, M. Tomaselli, T. Kühl, A. N. Artemyev, and V. A. Yerokhin, Phys. Rev. A **56**, 252 (1997).

[19] V. M. Shabaev, M. B. Shabaeva, I. I. Tupitsyn, V. A. Yerokhin, A. N. Artemyev, T. Kühl, M. Tomaselli, and O. M. Zherebtsov, Phys. Rev. A **57**, 149 (1998).

[20] V. M. Shabaev, M. B. Shabaeva, I. I. Tupitsyn, V. A. Yerokhin, A. N. Artemyev, T. Kühl, M. Tomaselli, and O. M. Zherebtsov, Phys. Rev. A **58**, 1610 (1998).

[21] M. G. H. Gustavsson and A.-M. Mårtensson-Pendrill, Phys. Rev. A **58**, 3611 (1998).

[22] P. Sunnergren, H. Persson, S. Salomonson, S. M. Schneider, I. Lindgren, and G. Soff, Phys. Rev. A **58**, 1055 (1998).

[23] V. M. Shabaev, M. B. Shabaeva, I. I. Tupitsyn, and V. A. Yerokhin, Hyperfine Interact. **114**, 129 (1998).

[24] M. B. Shabaeva and V. M. Shabaev, Phys. Rev. A **52**, 2811 (1995).

[25] G. Breit, Nature (London) **122**, 649 (1928).

[26] J. Schwinger, Phys. Rev. **73**, 416 (1948).

[27] J. Schwinger, Phys. Rev. **76**, 790 (1949).

[28] P. Kusch and H. M. Foley, Phys. Rev. **72**, 1256 (1947).

[29] H. M. Foley and P. Kusch, Phys. Rev. **73**, 412 (1948).

[30] R. Karplus and N. M. Kroll, Phys. Rev. **77**, 536 (1950).

[31] A. Petermann, Helv. Phys. Acta **30**, 407 (1957).

[32] C. M. Sommerfield, Ann. Phys. (N.Y.) **5**, 26 (1958).

[33] S. Laporta and E. Remiddi, Phys. Lett. B **379**, 283 (1996).

[34] V. W. Hughes and T. Kinoshita, Rev. Mod. Phys. **71**, S133 (1999).

[35] A.-M. Jeffrey, R. E. Elmquist, L. H. Lee, and R. F. Dziuba, IEEE Trans. Inst. Meas. **46**, 264 (1997).

[36] R. S.Van Dyck, Jr., P. B. Schwinberg, and H. G. Dehmelt, Phys. Rev. Lett. **59**, 26 (1987).

[37] H. Grotch, Phys. Rev. Lett. **24**, 39 (1970).

[38] H. Grotch, Phys. Rev. A **2**, 1605 (1970).

[39] H. Grotch and R. A. Hegstrom, Phys. Rev. A **4**, 59 (1971).

[40] R. Faustov, Nuovo Cimento A **69**, 37 (1970).

[41] R. Faustov, Phys. Lett. **33B**, 422 (1970).

[42] F. E. Close and H. Osborn, Phys. Lett. **34B**, 400 (1971).

[43] L. C. Balling and F. M. Pipkin, Phys. Rev. A **139**, A19 (1965).

[44] F. G. Walther, W. D. Phillips, and D. Kleppner, Phys. Rev. Lett. **28**, 1159 (1972).

[45] J. S. Tiedeman and H. G. Robinson, Phys. Rev. Lett. **39**, 602 (1977).

[46] C. E. Johnson and H. G. Robinson, Phys. Rev. Lett. **45**, 250 (1980).

[47] K. Hermanspahn, W. Quint, S. Stahl, M. Tönges, G. Bollen, H.-J. Kluge, R. Ley, R. Mann, and G. Werth, Acta Phys. Pol. B **27**, 357 (1996).

[48] M. Diederich, H. Häffner, N. Hermanspahn, M. Immel, H. J. Kluge, R. Ley, R. Mann, S. Stahl, W. Quint, J. Verdú, and G. Werth, in *Trapped Charged Particles and Fundamental Physics*, edited by D. H. E. Dubin and D. Schneider, AIP Conference Proc. No. 457 (AIP, Woodbury, NY, 1999), pp. 43–51.

[49] N. Hermanspahn, H. Häffner, H.-J. Kluge, W. Quint, S.

Stahl, J. Verdú, and G. Werth, Phys. Rev. Lett. (to be published).
[50] S. A. Blundell, K. T. Cheng, and J. Sapirstein, Phys. Rev. A **55**, 1857 (1997).
[51] H. Persson, S. Salomonson, P. Sunnergren, and I. Lindgren, Phys. Rev. A **56**, R2499 (1997).
[52] T. Beier, I. Lindgren, H. Persson, S. Salomonson, and P. Sunnergren, Hyperfine Interact. (to be published).
[53] V. M. Shabaev, Can. J. Phys. **76**, 907 (1998).
[54] S. S. Schweber, *An Introduction to Relativistic Quantum Field Theory* (Row, Peterson and Company, Evanston, IL, 1961).
[55] H. Margenau, Phys. Rev. **57**, 383 (1940).
[56] M. E. Rose, *Relativistic Electron Theory* (Wiley, New York, 1961).
[57] J. Sucher, Phys. Rev. **107**, 1448 (1957).
[58] M. Gell-Mann and F. Low, Phys. Rev. **84**, 350 (1951).
[59] P. J. Mohr, Phys. Rev. A **32**, 1949 (1985).
[60] L. Labzowsky, G. Klimchitskaya, and Y. Y. Dmitriev, *Relativistic Effects in the Spectra of Atomic Systems* (Institute of Physics Publishing, Bristol, 1993).
[61] I. Lindgren, in *Relativistic, Quantum Electrodynamic, and Weak Interaction Effects in Atoms*, edited by W. Johnson, P. Mohr, and J. Sucher, AIP Conf. Proc. No. 189 (AIP, New York, 1989), pp. 371–392.
[62] I. Lindgren, Phys. Scr. **T34**, 36 (1991).
[63] C. Itzykson and J. Bernard Zuber, *Quantum Field Theory* (McGraw-Hill, New York, 1980).
[64] G. C. Wick, Phys. Rev. **80**, 268 (1950).
[65] V. M. Shabaev and I. G. Fokeeva, Phys. Rev. A **49**, 4489 (1994).
[66] G. Soff and P. Mohr, Phys. Rev. A **38**, 5066 (1988).
[67] H. Persson, I. Lindgren, S. Salomonson, and P. Sunnergren, Phys. Rev. A **48**, 2772 (1993).
[68] I. Lindgren, H. Persson, S. Salomonson, V. Karasiev, L. Labzowsky, A. Mitrushenkov, and M. Tokman, J. Phys. B **26**, L503 (1993).
[69] I. Lindgren, H. Persson, and S. Salomonson, Phys. Rev. A **51**, 1167 (1995).
[70] I. Lindgren, H. Persson, S. Salomonson, and P. Sunnergren, Phys. Rev. A **58**, 1001 (1998).
[71] H. Persson, S. Salomonson, P. Sunnergren, and I. Lindgren, Phys. Rev. Lett. **76**, 204 (1996).
[72] H. Persson, S. M. Schneider, W. Greiner, G. Soff, and I. Lindgren, Phys. Rev. Lett. **76**, 1433 (1996).
[73] P. Indelicato and P. J. Mohr, Theor. Chim. Acta **80**, 207 (1991).
[74] N. J. Snyderman, Ann. Phys. (N.Y.) **211**, 43 (1991).
[75] M. Baranger, H. A. Bethe, and R. P. Feynman, Phys. Rev. **92**, 482 (1953).
[76] H. Persson, I. Lindgren, and S. Salomonson, Phys. Scr. Rev. **T46**, 125 (1993).
[77] T. Beier, G. Plunien, M. Greiner, and G. Soff, J. Phys. B **30**, 2761 (1997).
[78] A. N. Artemyev, V. M. Shabaev, and V. A. Yerokhin, Phys. Rev. A **56**, 3529 (1997).
[79] W. Pauli and F. Villars, Rev. Mod. Phys. **21**, 434 (1949).
[80] J. D. Bjorken and S. D. Drell, *Relativistic Quantum Mechanics* (McGraw-Hill, New York, 1964).
[81] E. A. Uehling, Phys. Rev. **48**, 55 (1935).
[82] R. C. Barrett, S. J. Brodsky, G. W. Erickson, and M. H. Goldhaber, Phys. Rev. **166**, 1589 (1968).
[83] J. Blomkvist, Nucl. Phys. **B48**, 95 (1972).
[84] K.-N. Huang, Phys. Rev. A **14**, 1311 (1976).
[85] S. Klarsfeld, Phys. Lett. **66B**, 86 (1977).
[86] D. J. Hylton, Phys. Rev. A **32**, 1303 (1985).
[87] M. Gyulassy, Nucl. Phys. A **244**, 497 (1975).
[88] H. Persson, Ph.D. thesis, Department of Physics, Göteborg University and Chalmers University of Technology, SE-41296 Göteborg, 1993.
[89] A. N. Artemyev, T. Beier, G. Plunien, V. M. Shabaev, G. Soff, and V. A. Yerokhin, Phys. Rev. A **60**, 45 (1999).
[90] W. H. Furry, Phys. Rev. **51**, 125 (1937).
[91] W. Greiner, B. Müller, and J. Rafelski, *Quantum Electrodynamics of Strong Fields* (Springer-Verlag, Berlin, 1985).
[92] S. A. Blundell, Phys. Rev. A **46**, 3762 (1992).
[93] V. A. Yerokhin and V. M. Shabaev, Phys. Rev. A **60**, 800 (1999).
[94] I. Lindgren and J. Morrison, *Atomic Many-Body Theory*, 2nd ed. (Springer-Verlag, Berlin, 1986).
[95] S. M. Schneider, Ph. D. thesis, Johann Wolfgang Goethe-Universität, Frankfurt am Main, Germany, 1995 (in German).
[96] S. Salomonson and P. Öster, Phys. Rev. A **40**, 5548 (1989).
[97] P. Sunnergren, Ph. D. dissertation, Göteborgs Universitet och Chalmers Tekniska Högskola, Department of Experimental Physics, Göteborg University and Chalmers University of Technology, SE–412 96 Göteborg, Sweden, 1998.
[98] I. Lindgren, H. Persson, S. Salomonson, and A. Ynnerman, Phys. Rev. A **47**, R4555 (1993).
[99] E. H. Wichmann and N. M. Kroll, Phys. Rev. A **101**, 843 (1956).
[100] E. Borie and G. A. Rinker, Rev. Mod. Phys. **54**, 67 (1982).
[101] T. Beier, P. J. Mohr, H. Persson, and G. Soff, Phys. Rev. A **58**, 954 (1998).
[102] V. M. Shabaev, J. Phys. B **26**, 1103 (1993).
[103] G. Fricke, C. Bernhardt, K. Heilig, L. A. Schaller, L. Schellenberg, E. B. Schera, and C. W. de Jager, At. Data Nucl. Data Tables **60**, 177 (1995).
[104] P. J. Mohr and G. Soff, Phys. Rev. Lett. **70**, 158 (1993).
[105] A. N. Artemyev, V. M. Shabaev, and V. A. Yerokhin, Phys. Rev. A **52**, 1884 (1995).
[106] V. M. Shabaev, A. N. Artemyev, T. Beier, G. Plunien, V. A. Yerokhin, and G. Soff, Phys. Rev. A **57**, 4235 (1998).
[107] G. Plunien and G. Soff, Phys. Rev. A **51**, 1119 (1995).
[108] G. Plunien and G. Soff, Phys. Rev. A **53**, 4614 (E) (1996).
[109] L. N. Labzowsky, A. V. Nefiodov, G. Plunien, T. Beier, and G. Soff, J. Phys. B **29**, 3841 (1996).
[110] A. V. Nefiodov, L. N. Labzowsky, G. Plunien, and G. Soff, Phys. Lett. A **222**, 227 (1996).
[111] G. Plunien, B. Müller, W. Greiner, and G. Soff, Phys. Rev. A **39**, 5428 (1989).
[112] G. Plunien, B. Müller, W. Greiner, and G. Soff, Phys. Rev. A **43**, 5853 (1991).
[113] T. Beier, M. Beinker, E. Persson, S. Zschocke, and G. Soff, Hyperfine Interact. **114**, 3 (1998).
[114] P. J. Mohr, in *Atomic, Molecular and Optical Physics Handbook*, edited by G. W. F. Drake (AIP, Woodbury, NY, 1996), Chap. 28, pp. 341–351.

[115] S. Mallampalli and J. Sapirstein, Phys. Rev. A **57**, 1548 (1998).

[116] T. Beier, P. J. Mohr, H. Persson, G. Plunien, M. Greiner, and G. Soff, Phys. Lett. A **236**, 329 (1997).

[117] J. D. Zumbro, E. B. Shera, Y. Tanaka, C. E. Bemis, Jr., R. A. Naumann, M. V. Hoehn, W. Reuter, and R. M. Steffen, Phys. Rev. Lett. **53**, 1888 (1984).

[118] J. D. Zumbro, R. A. Naumann, M. V. Hoehn, W. Reuter, E. B. Shera, C. E. Bemis, Jr., and Y. Tanaka, Phys. Lett. **167B**, 383 (1986).

[119] H. de Vries, C. W. de Jager, and C. de Vries, At. Data Nucl. Data Tables **36**, 495 (1987).

[120] H. Winter, S. Borneis, A. Dax, S. Faber, T. Kühl, D. Marx, F. Schmitt, P. Seelig, W. Seelig, V. M. Shabaev, M. Tomaselli, and M. Würtz, in *GSI Scientific Report 1998*, edited by U. Grundinger (GSI, Darmstadt, Germany, 1999), p. 87.

[121] S. M. Schneider, W. Greiner, and G. Soff, Z. Phys. D: At., Mol. Clusters **31**, 143 (1994).

[122] W. Quint (private communication).